


TRIM27 elicits protective immunity against tuberculosis by activating TFEB-mediated autophagy flux

Dongdong Zhao, Lihua Qiang, Zehui Lei, Pupu Ge, Zhe Lu, Yiru Wang, Xinwen Zhang, Yuyun Qiang, Bingxi Li, Yu Pang, Lingqiang Zhang, Cui Hua Liu & Jing Wang


To cite this article: Dongdong Zhao, Lihua Qiang, Zehui Lei, Pupu Ge, Zhe Lu, Yiru Wang, Xinwen Zhang, Yuyun Qiang, Bingxi Li, Yu Pang, Lingqiang Zhang, Cui Hua Liu & Jing Wang (04 Mar 2024): TRIM27 elicits protective immunity against tuberculosis by activating TFEB-mediated autophagy flux, *Autophagy*, DOI: [10.1080/15548627.2024.2321831](https://doi.org/10.1080/15548627.2024.2321831)


To link to this article: <https://doi.org/10.1080/15548627.2024.2321831>

 View supplementary material [↗](#)

 Published online: 04 Mar 2024.

 Submit your article to this journal [↗](#)

 Article views: 136

 View related articles [↗](#)

 View Crossmark data [↗](#)

RESEARCH PAPER



TRIM27 elicits protective immunity against tuberculosis by activating TFEB-mediated autophagy flux

Dongdong Zhao^{a,b,*}, Lihua Qiang^{a*}, Zehui Lei^{a,b*}, Pupu Ge^{a*}, Zhe Lu^{a,b}, Yiru Wang^{a,b}, Xinwen Zhang^{a,b}, Yuyun Qiang^{a,b}, Bingxi Li^a, Yu Pang^c, Lingqiang Zhang^d, Cui Hua Liu^{a,b}, and Jing Wang^a

^aCAS Key Laboratory of Pathogenic Microbiology and Immunology, Institute of Microbiology, Chinese Academy of Sciences, Beijing, China; ^bSavaid Medical School, University of Chinese Academy of Sciences, Beijing, China; ^cBeijing Tuberculosis and Thoracic Tumor Research Institute, Beijing Chest Hospital, Capital Medical University, Beijing, China; ^dState Key Laboratory of Proteomics, National Center for Protein Sciences (Beijing), Beijing Institute of Lifeomics, Beijing, China

ABSTRACT

Infectious diseases, such as *Mycobacterium tuberculosis* (Mtb)-caused tuberculosis (TB), remain a global threat exacerbated by increasing drug resistance. Host-directed therapy (HDT) is a promising strategy for infection treatment through targeting host immunity. However, the limited understanding of the function and regulatory mechanism of host factors involved in immune defense against infections has impeded HDT development. Here, we identify the ubiquitin ligase (E3) TRIM27 (tripartite motif-containing 27) as a host protective factor against Mtb by enhancing host macroautophagy/autophagy flux in an E3 ligase activity-independent manner. Mechanistically, upon Mtb infection, nuclear-localized TRIM27 increases and functions as a transcription activator of *TFEB* (transcription factor EB). Specifically, TRIM27 binds to the *TFEB* promoter and the TFEB transcription factor CREB1 (cAMP responsive element binding protein 1), thus enhancing CREB1-*TFEB* promoter binding affinity and promoting CREB1 transcription activity toward *TFEB*, eventually inducing autophagy-related gene expression as well as autophagy flux activation to clear the pathogen. Furthermore, TFEB activator 1 can rescue TRIM27 deficiency-caused decreased autophagy-related gene transcription and attenuated autophagy flux, and accordingly suppressed the intracellular survival of Mtb in cell and mouse models. Taken together, our data reveal that TRIM27 is a host defense factor against Mtb, and the TRIM27-CREB1-*TFEB* axis is a potential HDT-based TB target that can enhance host autophagy flux.

Abbreviations: ATG5: autophagy related 5; BMDMs: bone marrow-derived macrophages; CFU: colony-forming unit; ChIP-seq: chromatin immunoprecipitation followed by sequencing; CREB1: cAMP responsive element binding protein 1; CTSB: cathepsin B; E3: ubiquitin ligase; EMSA: electrophoretic mobility shift assay; HC: healthy control; HDT: host-directed therapy; LAMP: lysosomal associated membrane protein; MAP1LC3/LC3: microtubule associated protein 1 light chain 3; MCOLN1: mucolipin TPR cation channel 1; Mtb: *Mycobacterium tuberculosis*; NLS: nuclear localization signal; PBMCs: peripheral blood mononuclear cells; PRKA/PKA: protein kinase cAMP-activated; qRT-PCR: quantitative real-time PCR; RFP: RET finger protein; TB: tuberculosis; TBK1: TANK binding kinase 1; TFEB: transcription factor EB; TRIM: tripartite motif; TSS: transcription start site; ULK1: unc-51 like autophagy activating kinase 1.

ARTICLE HISTORY

Received 29 August 2023
Revised 27 January 2024
Accepted 16 February 2024

KEYWORDS

Autophagy flux; cAMP responsive element binding protein 1; *Mycobacterium tuberculosis*; transcription factor EB; tripartite motif-containing 27; tuberculosis

Introduction


Tuberculosis (TB), which is caused by *Mycobacterium tuberculosis* (Mtb), remains one of the main causes of death from infectious diseases, with approximately 10 million new cases and 1.5 million deaths each year [1]. Over the past decades, antibiotics targeting Mtb have greatly improved treatment outcomes in patients with drug-susceptible TB. However, the widespread emergence of drug-resistant TB cases, especially rifampicin-resistant/RR, multidrug-resistant/MDR and extensively drug-resistant/XDR TB cases [1], has rendered currently available drugs ineffective for patients with drug-resistant TB, further posing a huge challenge to global TB control [2]. Against this backdrop, World Health

Organization (WHO) recently released its global research agenda for antimicrobial resistance in human health, in which it outlines 40 research topics on drug-resistant bacteria including Mtb [3], thus complementing strategies improving drug-resistant TB treatment are urgently needed.

Recently, much effort has been made to develop novel/improved therapies by modulating host immune responses to TB, and host-directed therapy (HDT) strategies designed to enhance host protective immune responses, reduce exacerbated inflammation and balance immune reactivity have received increasing attention [4]. Unlike anti-TB drugs that directly target Mtb, HDTs possess the following potential advantages: first, HDTs can be effective against both drug

CONTACT Jing Wang ✉ wangj6@im.ac.cn; Cui Hua Liu ✉ liucuihua@im.ac.cn CAS Key Laboratory of Pathogenic Microbiology and Immunology, Institute of Microbiology, Chinese Academy of Sciences, Beijing 100101, China

*These authors contributed equally to this work.

 Supplemental data for this article can be accessed online at <https://doi.org/10.1080/15548627.2024.2321831>

© 2024 Informa UK Limited, trading as Taylor & Francis Group

-susceptible and drug-resistant Mtb; second, HDTs are less likely to induce Mtb drug resistance; third, HDTs could shorten the duration of antibiotic treatment by targeting a variety of components/pathways of the host immune system [5]. A number of clinical trials of HDTs for TB are generally fall into two categories: cytokine-based therapies for augmenting immunity to eradicate infection (such as IFNG/IFN- γ (interferon gamma) and IL2 (interleukin 2) administration) and strategies for ameliorating pathology to prevent permanent tissue injury (such as type I interferon blockade), but most of these HDT candidates have shown only limited promise in certain conditions or have proven to be detrimental [6]. Thus, seeking more effective HDT targets against infections, especially the intractable and chronic infectious diseases such as TB, has become a research hotspot. Increasing studies have indicated that triggering host innate immune defense mechanisms is a promising HDT strategy for TB treatment [4]. For example, macroautophagy/autophagy, an efficient innate immune response restricting Mtb intracellular survival, represents an attractive target for HDT to combat Mtb infection [7]. Therefore, identifying critical host factors involved in these innate immune processes could provide more effective HDT targets that could complement current treatment protocols [8]. However, the host factors and their regulatory mechanisms involved in host immune defense against Mtb are largely unexplored.

Tripartite motif (TRIM) family proteins represent one of the largest classes of the Really Interesting New Gene (RING)-type ubiquitin ligases (E3s), which contain more than 80 members and are divided into 11 sub-groups based on the variable domain present at the C terminus, including C-I to C-XI sub-groups and a unclassified (UC) subgroup, of which the C-IV subgroup is the largest one consisting of over 30 members [9]. TRIM proteins are involved in a broad range of cellular processes and functions including transcriptional regulation, protein modification and homeostasis, cell proliferation, apoptosis and autophagy, in a manner dependent or independent on their E3 ligase activity, thereby controlling host immune defense against diseases, such as infectious diseases [10,11]. Previous studies primarily reported regulatory mechanisms of TRIM proteins in host antiviral immunity through modulating host interferon signaling and autophagy pathways [12,13]. Recently, several studies have revealed the regulatory roles of TRIM proteins in infections caused by bacteria such as Mtb. For example, during Mtb infection, TRIM16 induces the activation of selective autophagy through assembling core autophagy factors and influencing MTOR (mechanistic target of rapamycin kinase) and TFEB activity [14], TRIM32 promotes both the recruitment of BECN1/Beclin 1 to Mtb and the phagophore engulfment of Mtb [15], TRIM22 augments autophagy via the NFKB/NF- κ B (nuclear factor kappa B)-BECN1 pathway and participates in autolysosomal biogenesis [16], and TRIM14 localizes to Mtb-containing autophagosomes to modulate bacterial survival [17]. Therefore, TRIM proteins are potent critical host factors regulating Mtb infection, identifying the TRIM protein involved in host anti-Mtb immunity and revealing the underlying molecular mechanisms will provide promising strategies and potential targets for HDT of TB.

In this study, by comparing the gene expression of TRIM C-IV sub-group, the largest one of the TRIM family, in peripheral blood mononuclear cells (PBMCs) from healthy control (HC) individuals or TB patients, we found that *TRIM27* gene transcription is the most significantly reduced in TB patients as compared with that in HC group. Through further conducting Mtb infection experiments, we demonstrated that, upon Mtb infection, the level of nuclear TRIM27 increases and then functions as a transcription activator to promote the transcription of *TFEB* (transcription factor EB). Specifically, TRIM27 not only binds to the promoter region of *TFEB*, but also interacts with the *TFEB* transcription factor CREB1 (cAMP responsive element binding protein 1), thus increasing the affinity of CREB1 to the *TFEB* promoter and promoting PRKA/protein kinase A-catalyzed CREB1 phosphorylation and activation, eventually enhancing *TFEB* gene transcription and the ensuing autophagy-related gene expression and autophagy activation to clear Mtb. Furthermore, *TFEB* activator 1 can rescue the decreased transcription of autophagy-related genes, attenuated autophagy flux and reduced Mtb clearance in *Trim27*-deficient cell and mouse models. Together, our findings indicate that TRIM27 serves as a critical host protective factor against Mtb infection, suggesting a potential HDT-based TB treatment via targeting TRIM27-CREB1-TFEB axis.

Results

TRIM27 is a potential host protective factor against Mtb infection

TRIM family proteins, especially the C-IV sub-group, have been reported to play important regulatory roles in host antiviral defenses through modulating host interferon signaling pathways [18], but their functions in host defense against pathogenic bacteria are largely unexplored. Here, we collected PBMCs from HC individuals or patients with TB (Table S1), a serious chronic bacterial infectious disease caused by Mtb, for gene expression analysis to investigate the TRIM protein involved in host anti-Mtb immunity. Interestingly, we observed a total of 8 TRIM transcripts (*MID2/TRIM1*, *TRIM6*, *TRIM21*, *TRIM27*, *TRIM39*, *TRIM68*, *TRIM69* and *TRIM75*) decreased in TB patients in comparison with that in HC individuals, among which *TRIM27* showed the most significant reduction (Figure 1A,B; Table S2). We thus focused on TRIM27 to further investigate its functional roles in host anti-Mtb immunity. Through analyzing the expression of TRIM27 in different immune cell populations in PBMCs from HC or TB patients, we found that TRIM27 was highly expressed in monocytes, and the abundance of TRIM27 in monocytes from TB patients was significantly lower than that in monocytes from HC individuals (Figure 1C and S1A). Collectively, TRIM27 is lowly expressed in monocytes from TB patients.

To further investigate whether low expression of TRIM27 in monocytes affects host anti-Mtb immunity, we established *Trim27^{fllox/fllox} (Trim27^{fl/fl})-Lyz2/LyzM^{Cre} (trim27^{-/-})* mice with TRIM27 deficiency in myeloid cell lineage (monocytes,

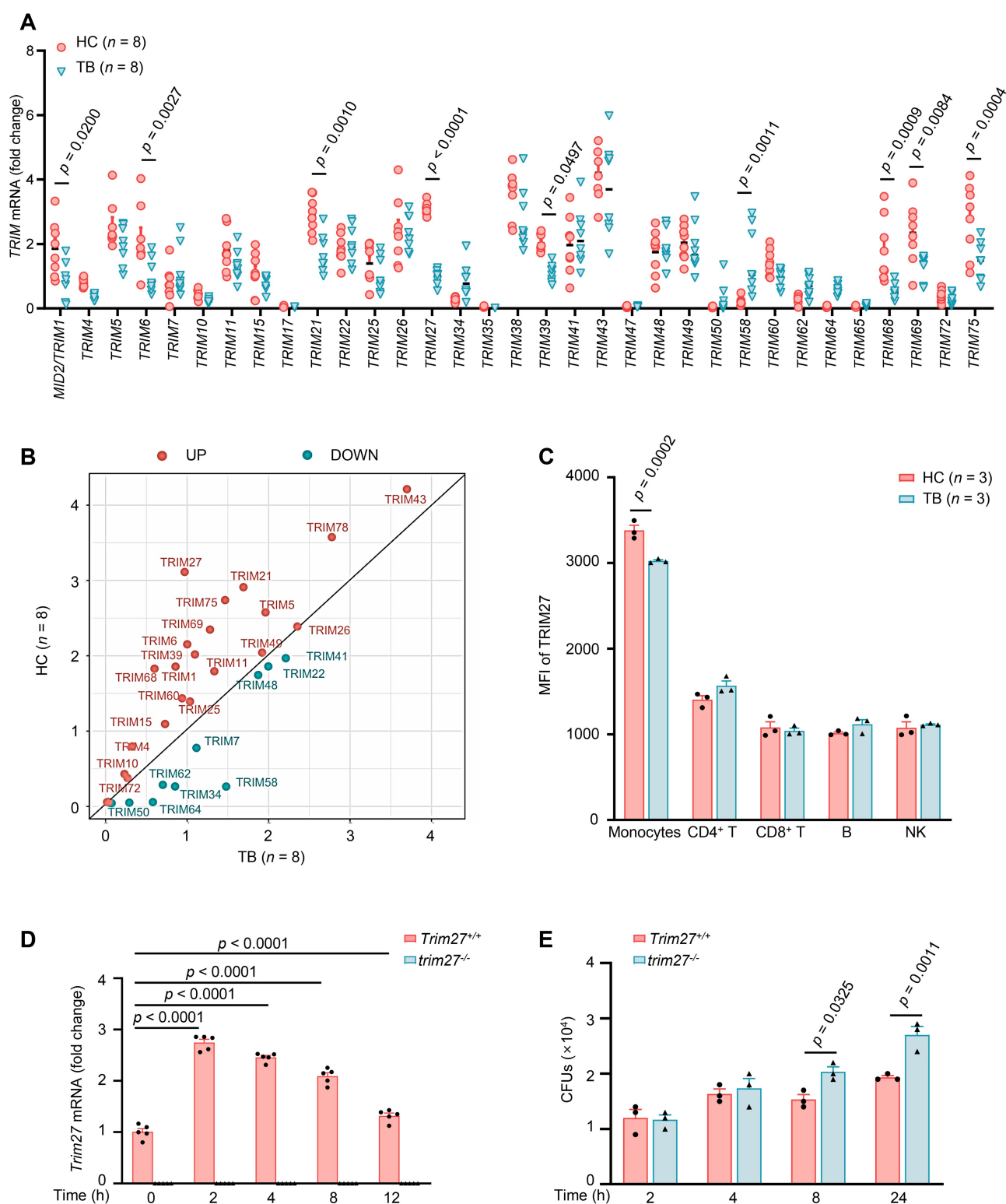


Figure 1. TRIM27 is a potential host protective factor against mtb infection. (A) expression profiling of the C-IV TRIM family proteins in PBMCs from healthy control (HC) ($n = 8$) and TB patients ($n = 8$). (B) scatter map showing the differential expression of C-IV TRIM family genes in PBMCs from HC ($n = 8$) and TB ($n = 8$). (C) the expression of TRIM27 in peripheral blood immune cells of HC ($n = 3$) and TB ($n = 3$) groups as determined by fluorescence-activated cell sorting (FACS). MFI, mean fluorescence intensity. (D) quantitative real-time PCR (qRT-PCR) analysis of *Trim27* mRNA in *Trim27^{+/+}* and *trim27^{-/-}* BMDMs. Cells were infected with mtb at a MOI of 5 for 0–12 h, and results are presented relative to those of the control gene *Gapdh*. (E) survival of mtb in *Trim27^{+/+}* and *trim27^{-/-}* BMDMs. Cells were infected as in (D) for 0–24 h. Data are mean \pm SEM ($n = 5$ replicates per group in D and $n = 3$ replicates per group in E). Statistical significance was determined using two-way ANOVA with Sidak's multiple comparisons test for (A, C and E) and two-way ANOVA with Tukey's post-hoc test for (D). Results are representative of three independent experiments.

mature macrophages and granulocytes) to investigate the function and mechanism of TRIM27 in host defense against Mtb (Figure S1B – D). We found that the expression of *Trim27* was significantly elevated in bone marrow-derived macrophages (BMDMs) collected from *Trim27^{fl/fl}* mice (*Trim27^{+/+}* BMDMs) upon Mtb infection, followed by a decline after 4 h post-infection, while the expression of *Trim27* was not detected in BMDMs of *trim27^{-/-}* mice (Figure 1D). Then, we further investigated the specific component of Mtb contributing to upregulated TRIM27 expression. Through digesting DNA, RNA or proteins of Mtb with the indicated enzymes and degrading carbohydrate residues of Mtb with NaIO₄, and we found that Mtb lacking carbohydrate residues abolished its ability to promote *TRIM27* transcription during Mtb infection (Figure S2A). Subsequently, we removed peptidoglycan, lipomannan and lipoarabinomannan carbohydrate chains from the Mtb cell-wall fractions, and identified that lipomannan and lipoarabinomannan are critical determinants to induce *TRIM27* mRNA expression (Figure S2B). Finally, Mtb colony-forming unit (CFU) assay showed that *trim27^{-/-}* BMDMs exhibited much weaker effects on clearing Mtb than *Trim27^{+/+}* BMDMs (Figure 1E). Together, these results indicate that TRIM27 is a potential host protective factor in response to Mtb infection, and the low expression of TRIM27 in monocyte-derived macrophages/MDMs may lead to TB occurrence and progression.

Nuclear-localized TRIM27 increases to enhance TFEB gene transcription under Mtb infection

Next, we sought to investigate the underlying mechanism by which TRIM27 contributes to host anti-Mtb immunity. Our previous study has revealed that TRIM27 in the cytosol can modulate the activation of innate immune signaling pathways, including NFκB/NF-κB and MAPK/p38 (mitogen-activated protein kinase) pathways, to suppress the intracellular survival of mycobacteria Bacille Calmette-Guerin (BCG) [19]. In this study, we noticed that the TRIM27 protein levels in the cytoplasm and nucleus significantly increased in Mtb-infected BMDMs than that in uninfected controls (Figure 2A–C). To gain new insights into whether and how nuclear TRIM27 regulates host defense against Mtb, chromatin immunoprecipitation followed by sequencing (ChIP-seq) analysis using TRIM27-specific antibody was conducted in HC PBMCs with or without Mtb infection. A total of 58 TRIM27-specific ChIP-seq signals were examined in uninfected PBMCs, of which 37 (63.79%) were located in intergenic regions, 16 (27.59%) were located in intron regions and 2 (3.45%) were located in promoter regions (Figure 2D). Meanwhile, a total of 4906 TRIM27-specific ChIP-seq signals were examined in Mtb-infected PBMCs, of which 2986 (60.86%) were located in intergenic regions, 1753 (35.73%) were located in intron regions and 106 (2.16%) were located in promoter regions (Figure 2D). In addition, among the potential TRIM27-targeting sites analyzed, 56.90% protein-coding associated regions and 39.66% noncoding RNAs (ncRNAs) were identified in uninfected PBMCs, as well as 68.02% protein-coding associated regions and 30% ncRNAs were identified in Mtb-infected PBMCs (Figure 2E),

indicating that TRIM27 mainly targets protein-coding associated regions. Then, we further analyzed the differential protein-coding-associated regions potentially targeted by TRIM27 in uninfected and Mtb-infected PBMCs. Among 3374 such regions, 72 (2.13%) were present within 3 kb from the transcription start site (TSS) of known RefSeq genes (Table S3), of which 16 TRIM27-targeted candidates with fold-enrichment >10 and false discovery rate (FDR) < 0.05 were screened out (Figure 2F).

We next performed quantitative real-time PCR (qRT-PCR) using PBMCs with or without Mtb infection to verify the ChIP-seq data, and confirmed that the transcription of several TRIM27-targeted candidates, including *TFEB*, *MYDGF/C19orf10* (myeloid derived growth factor) and *LCE1A* (late cornified envelope 1A), were significantly elevated in cells infected with Mtb ($p < 0.0001$), among which *TFEB* showed the most significant upregulation (Figure 3A). We then used *Trim27^{+/+}* and *trim27^{-/-}* BMDMs to examine the transcriptional level of *Tfeb* during Mtb infection. *Trim27^{+/+}* BMDMs showed an increase of *Tfeb* transcription at 4 h post-infection, followed by a decline after 8 h, while this phenomenon was abolished in *trim27^{-/-}* BMDMs (Figure 3B), confirming that TRIM27 contributes to the transcription of *TFEB* gene during Mtb infection. Consistently, PBMCs from TB patients with lower *TRIM27* expression showed downregulated *TFEB* transcription, comparing with that from HC individuals (Figure 3C), suggesting a positive correlation between *TRIM27* expression and *TFEB* transcription in clinical. Furthermore, ChIP-qPCR assay demonstrated that TRIM27 was highly enriched in the promoter region of *TFEB* gene under Mtb infection (Figure 3D). To further confirm the direct regulatory roles of TRIM27 on *TFEB* gene transcription, we inserted the promoter region of *TFEB* into the pGL2-Basic vector to construct a reporter plasmid, and then performed luciferase reporter assays in HEK293T cells co-transfected with the reporter plasmid and plasmid encoding TRIM27, and the result showed that TRIM27 could significantly induce the transcription of *TFEB* gene (Figure 3E). Consistently, we also confirmed that TRIM27 promoted *TFEB* protein expression (Figure S3A). Moreover, through extracting the cytoplasmic and nuclear fractions of *Trim27^{+/+}* and *trim27^{-/-}* BMDMs, we found that the *TFEB* abundance both in the cytoplasm and nucleus significantly increased in *Trim27^{+/+}* BMDMs upon Mtb infection compared with that in *trim27^{-/-}* BMDMs, while the ratio of nuclear:cytoplasmic *TFEB* per cell remained unchanged both in *Trim27^{+/+}* and *trim27^{-/-}* BMDMs during Mtb infection (Figure S3B, C). Collectively, Mtb infection induces the upregulation of nuclear-localized TRIM27 to promote *TFEB* expression.

Nuclear TRIM27 promotes TFEB-mediated activation of autophagy

TFEB, a member of the MiTF (microphthalmia-transcription factor)/TFE family of leucine zipper transcription factors, plays a critical regulatory role in promoting the transcription of a series of autophagy- and lysosomal biogenesis-related genes, including *MAP1LC3/LC3* (microtubule associated protein 1 light chain 3), *SQSTM1/p62* (sequestosome 1), *CTSB* (cathepsin B), *ATG5* (autophagy related 5), *MCOLN1*

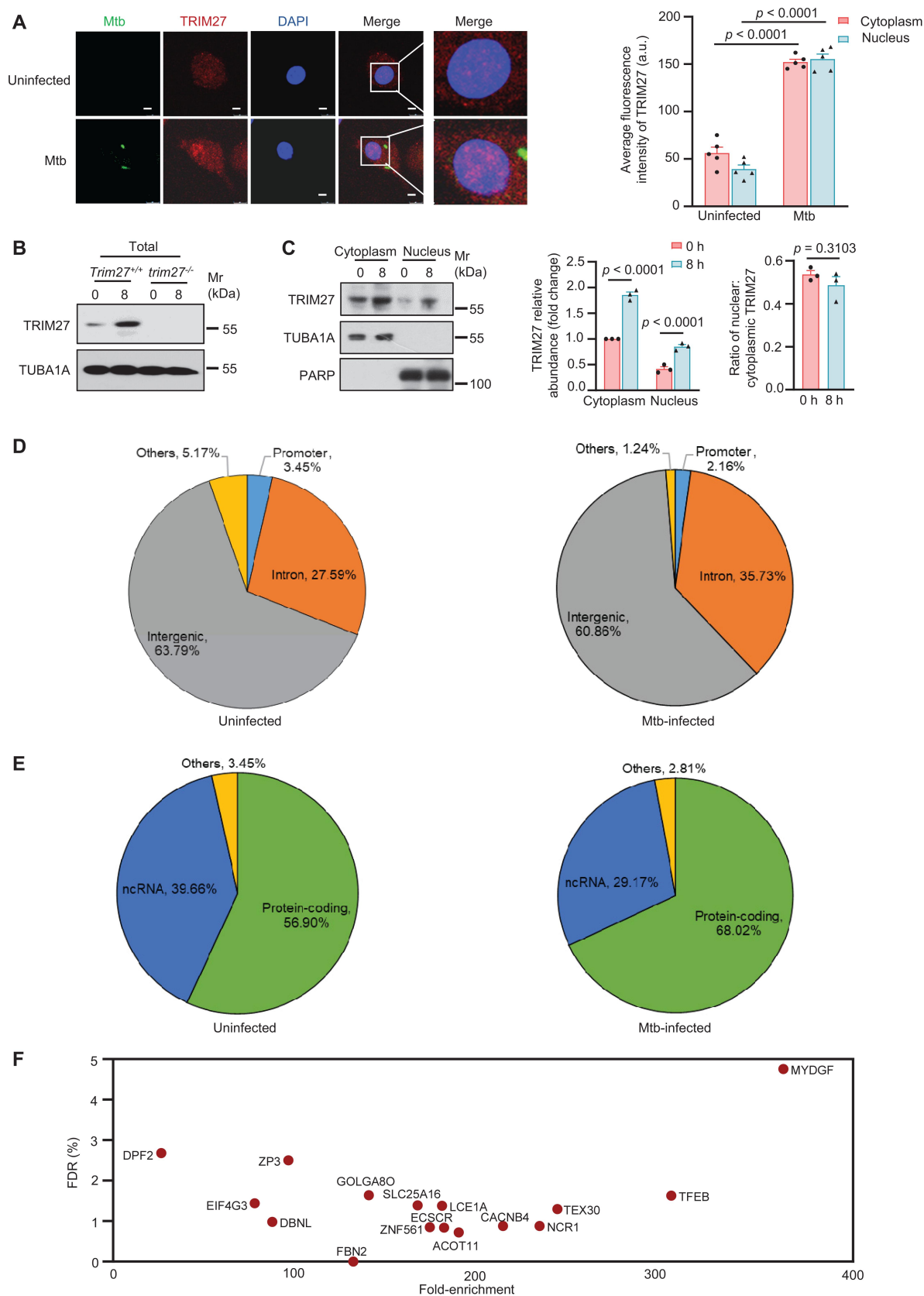


Figure 2. TRIM27 nuclear localization increases upon mtb infection. (A) confocal microscopy analysis of the nuclear localization of TRIM27. Left, Representative confocal images of the colocalization of TRIM27 and the nucleus in HC PBMCs. Cells were uninfected or infected with Alexa Fluor™ 488-labeled mtb (green) at a MOI of 5 for 8 h, and were then fixed and stained with the antibody against TRIM27 (red). Nuclei were stained with DAPI (blue). Scale bars: 10 μ m. Right, average fluorescence intensity of TRIM27 in the cytoplasm and nucleus from HC PBMCs. About 50 cells were counted and analyzed for each biological replicate. (B) immunoblotting of total TRIM27 and TUBA1A (loading control) in *Trim27*^{+/+} and *trim27*^{-/-} BMDMs. Cells were infected with mtb strains at a MOI of 5 for 0–8 h. (C) immunoblotting of TRIM27, TUBA1A (loading control for the cytoplasm) and PARP (loading control for the nucleus) in the cytoplasm and the nucleus from *Trim27*^{+/+} BMDMs (left). Cells were infected as in (B). Middle, the relative abundance of TRIM27 in the cytoplasm and nucleus from *Trim27*^{+/+} BMDMs. Right, the ratio

(mucolipin TPR cation channel 1), *LAMP1* (lysosomal associated membrane protein 1) and *LAMP2*, among which *MAP1LC3*, *SQSTM1* and *ATG5* encode critical factors in autophagy initiation, whereas *CTSB*, *MCOLN1*, *LAMP1* and *LAMP2* encode critical factors in lysosomal biogenesis [20–22]. We thus speculated whether TRIM27 increases TFEB-targeted autophagy- and lysosomal biogenesis-related gene expression to promote immune defense against bacterial infection. As expected, during Mtb infection, the transcription of *Map1lc3*, *Sqstm1*, *Ctsb*, *Atg5*, *Mcoln1*, *Lamp1* and *Lamp2* significantly increased in *Trim27^{+/+}* BMDMs, while the expression of these genes only slightly increased in *trim27^{-/-}* BMDMs (Figure 4A–G). Consistently, the protein levels of the 14-kDa lipidated autophagosome-bound form of MAP1LC3 (LC3-II) [23] significantly increased in *Trim27^{+/+}* BMDMs than that in *trim27^{-/-}* macrophages during Mtb infection, which difference was more significant in the presence of bafilomycin A₁, a proton ATPase inhibitor that prevents the lysosomal degradation by inhibiting the acidification of lysosomes [24] (Figure 4H). In addition, the number of MAP1LC3 puncta and the colocalization of Mtb with MAP1LC3-positive autophagosomes significantly increased in *Trim27^{+/+}* BMDMs than that in *trim27^{-/-}* macrophages upon Mtb infection (Figure S4A), suggesting that TRIM27 induces autophagy to sequester Mtb. Meanwhile, the fluorescence intensity of LysoTracker, a fluorescent probe indicating acidified lysosomes [25], and the expression of lysosomal membrane protein LAMP1, as well as the percentage of Mtb-LysoTracker and Mtb-LAMP1 colocalization were much higher in *Trim27^{+/+}* BMDMs than that in *trim27^{-/-}* BMDMs during Mtb infection (Figure S4B, C), suggesting that TRIM27 also contributes to lysosomal biogenesis and Mtb targeting to lysosomes. Taken together, TRIM27 increases TFEB-targeted autophagy- and lysosomal biogenesis-related gene expression to promote the activation of autophagy for Mtb clearance.

Autophagy undergoes phagophore formation, autophagosome formation, autophagosome-lysosome fusion and eventual cargo degradation, and the whole dynamic process is defined as autophagy flux [26]. To further explore the regulatory role of TRIM27 in modulating autophagy flux, we took advantage of the tandem mCherry-GFP-MAP1LC3 construct, which is detected as red puncta in autolysosomes and as yellow puncta in immature autophagosomes, for confocal microscopy experiments. Expectedly, the number of the total MAP1LC3 puncta per cell that represents the intensity of autophagosome formation was significantly higher, while the ratio of yellow:total puncta per cell that represents the ratio of immature autophagosomes was markedly lower, in *Trim27^{+/+}* BMDMs than that in *trim27^{-/-}* BMDMs with or without Mtb infection (Figure 4I). Thus, TRIM27 enhances autophagy flux during Mtb infection. Since unobstructed autophagy flux

contributes to the clearance of intracellular pathogens, we speculated that TRIM27 promotes Mtb clearance by enhancing autophagy flux. Through knocking out the core autophagy gene *Atg5* in *Trim27^{+/+}* and *trim27^{-/-}* macrophages to block autophagy (Figure S4D), we found that the promoting effect of TRIM27 on clearing Mtb was largely abolished (Figure S4E), indicating that TRIM27 enhances ATG5-dependent autophagy flux to achieve pathogen clearance during Mtb infection.

To further verify whether TRIM27 enhances autophagy flux depending on TFEB, we treated *Trim27^{+/+}* and *trim27^{-/-}* BMDMs with TFEB activator 1, which could activate TFEB by directly binding to TFEB and promoting its entry into the nucleus, without affecting *TFEB* transcription [27]. As expected, TFEB activator 1 rescued the decreased transcription of autophagy-related genes, including *Map1lc3*, *Sqstm1*, *Ctsb*, *Atg5*, *Mcoln1*, *Lamp1* and *Lamp2* (Figure S5A – G), without affecting the transcription of *Trim27* and *Tfeb* (Figure S5H, I). Consistently, TFEB activator 1 enhanced TRIM27 deficiency-caused attenuated autophagy flux (Figure S5J, K), and accordingly suppressed the intracellular survival of Mtb (Figure S5L). Additionally, previous studies have reported that TRIM27 restrains starvation-induced autophagy through impacting the ULK1 (unc-51 like autophagy activating kinase 1) complex or promoting mitophagy by recruiting active TBK1 (TANK binding kinase 1) to the mitochondria [28,29], we thus further determined whether TRIM27 modulates host autophagy during Mtb infection via these two mechanisms. Through examining the protein stability of ULK1 and the activation of its substrate ATG13 in *Trim27^{+/+}* and *trim27^{-/-}* BMDMs, we found that the protein levels of ULK1 and phosphorylated ATG13 (active ATG13) were similar between *Trim27^{+/+}* and *trim27^{-/-}* BMDMs during Mtb infection (Figure S5M). Moreover, we purified the mitochondria from *Trim27^{+/+}* and *trim27^{-/-}* BMDMs to examine the abundance of phosphorylated TBK1 (active TBK1) being recruited to the mitochondria during Mtb infection, and the result showed that Mtb infection can increase the abundance of phosphorylated TBK1 on the mitochondria, while this effect was not modulated by TRIM27 (Figure S5N). Taken together, these data indicate that TRIM27 enhances autophagy flux during Mtb infection in a manner depending on TFEB, rather than impacting the ULK1 complex or promoting the recruitment of active TBK1 to the mitochondria. Next, we further examined whether TRIM27 promotes *TFEB* transcription to induce autophagy flux in the nucleus. Through analyzing the amino acid sequence of TRIM27 using cNLS Mapper [30,31], we found an importin α -dependent nuclear localization signal (NLS) in TRIM27, which is located at the amino acid 152–164 (Figure 5A). Then, we constructed the NLS-deleted TRIM27 (TRIM27 Δ NLS) and confirmed that

of nuclear:cytoplasmic TRIM27. Densitometry of triplicate samples was performed for quantification. The relative abundance of TRIM27 in the cytoplasm and nucleus was calculated as the ratios of TRIM27:TUBA1A and the ratios of TRIM27:PARP, respectively. (D) genomic distribution of potential TRIM27-binding regions in HC PBMCs. Cells were infected as in (B). (E) biotype distribution of potential TRIM27-binding regions in HC PBMCs. Cells were infected as in (B). (F) the total 16 candidate protein-coding genes (fold-enrichment >10 and FDR <0.05) whose promoter region is regulated by TRIM27 in mtb-infected PBMCs. Data are mean \pm SEM ($n=5$ replicates per group in A and $n=3$ replicates per group in C). Statistical significance was determined using two-way ANOVA with Tukey's post-hoc test for (A), two-way ANOVA with Sidak's multiple comparisons test for (C, middle) and unpaired two-sided Student's *t*-test for (C, right). Results are representative of three independent experiments.

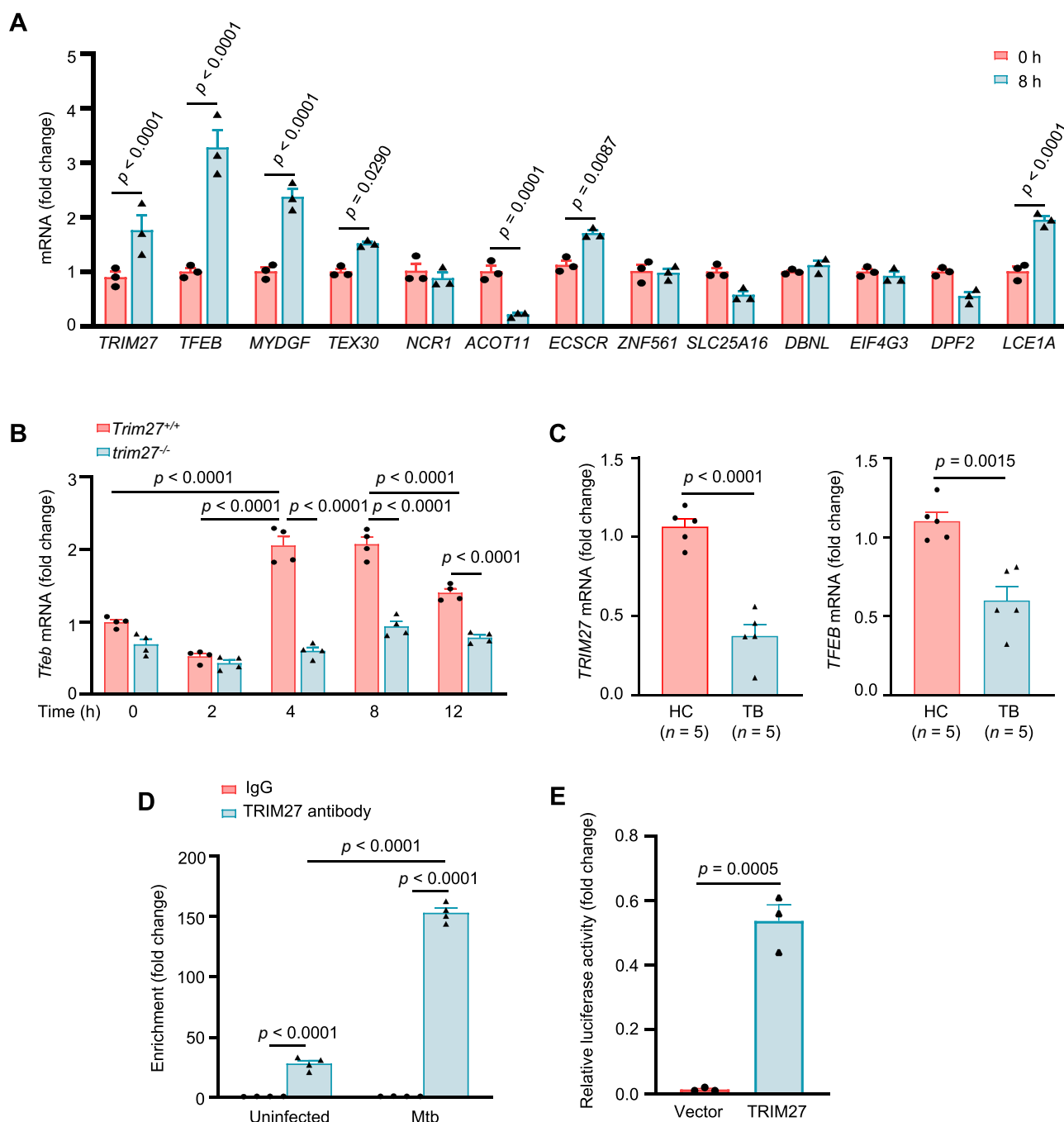


Figure 3. Nuclear TRIM27 promotes *TFEB* gene transcription. (A) qRT-PCR analysis of the potential genes targeted by TRIM27. The mRNA levels of potential TRIM27-targeted genes were determined in HC PBMCs infected with mtb at a MOI of 5 for 0 or 8 h. The copy numbers of mRNA were calculated based on the *GAPDH* standard curve. TEX30: testis expressed 30; NCR1: natural cytotoxicity triggering receptor 1; ACOT11: acyl-CoA thioesterase 11; ECSCR: endothelial cell surface expressed chemotaxis and apoptosis regulator; ZNF561: zinc finger protein 561; SLC25A16: solute carrier family 25 member 16; DBNL: drebrin like; EIF4G3: eukaryotic translation initiation factor 4 gamma 3; DPF2: double PHD fingers 2. (B) qRT-PCR analysis of *tfeb* mRNA in *Trim27*^{+/+} and *trim27*^{-/-} BMDMs. Cells were infected with mtb at a MOI of 5 for 0–12 h, and results are presented relative to those of the control gene *Gapdh*. (C) qRT-PCR analysis of *TRIM27* mRNA (left) and *TFEB* mRNA (right) in PBMCs from HC ($n = 5$) and TB ($n = 5$) individuals. Results are presented relative to those of the control gene *GAPDH*. (D) ChIP-qPCR assay for TRIM27 enrichment in the promoters of potential target gene *TFEB*. ChIP assay was conducted using anti-TRIM27 rabbit antibody followed by qRT-PCR in PBMCs uninfected or infected with mtb for 8 h. Enrichment was calculated relative to normal rabbit IgG control. (E) Luciferase reporter assay of the transcriptional regulation activity of TRIM27 on its potential target gene *TFEB* in HEK293T cells. *TFEB* promoter-pGL2-basic vector was co-transfected into HEK293T cells with 1 μ g of empty vector or vectors encoding full-length TRIM27. Resultant luciferase activities were expressed as relative luciferase activities normalized to the pRL-TK activity. Data are mean \pm SEM ($n = 3$ replicates per group in A and E, $n = 4$ replicates per group in B and D). Statistical significance was determined using two-way ANOVA with Sidak's multiple comparisons test for (A), two-way ANOVA with Tukey's post-hoc test for (B and D) and unpaired two-sided Student's *t*-test for (C and E). Results are representative of three independent experiments.

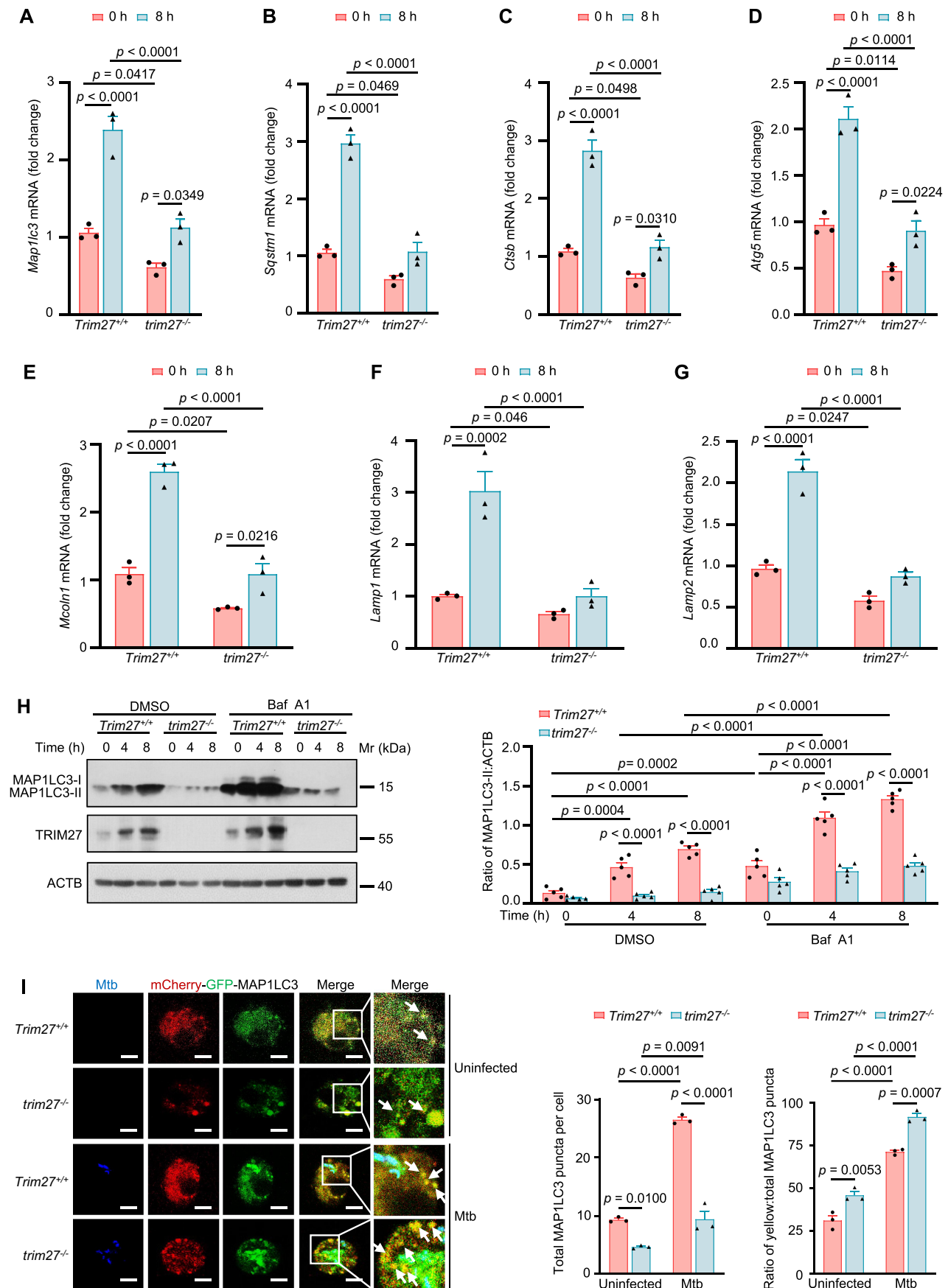


Figure 4. Nuclear TRIM27 promotes TFEB-mediated activation of autophagy. (A–G) qRT-PCR analysis of *Map1lc3* mRNA (A), *Sqstm1* mRNA (B), *ctsb* mRNA (C), *Atg5* mRNA (D), *Mcoln1* mRNA (E), *Lamp1* mRNA (F) and *Lamp2* mRNA (G) in *Trim27*^{+/+} and *trim27*^{-/-} BMDMs. Cells were infected with mtb at a MOI of 5 for 0 or 8 h, and results are presented relative to those of the control gene *Gapdh*. (H) Immunoblotting of MAP1LC3, TRIM27 and ACTB (loading control) in *Trim27*^{+/+} and *trim27*^{-/-} BMDMs. Cells were infected with mtb at a MOI of 5 for 0–8 h in the presence of DMSO or bafilomycin A1 (baf A1), and were then lysed and analyzed by

TRIM27 Δ NLS lost its ability to enter host cell nucleus upon Mtb infection (Figure 5B,C). Accordingly, TRIM27 Δ NLS largely lost its function of enhancing autophagy flux during Mtb infection, as compared with wild-type TRIM27 (Figure 5D). Altogether, these results indicate that TRIM27 enhances TFEB-activated autophagy flux to accelerate Mtb clearance, depending on its nuclear localization.

Nuclear TRIM27 functions as a transcription activator to enhance TFEB gene transcription during Mtb infection

To further investigate how TRIM27 promotes the transcription of *TFEB*, we amplified the promoter region (–1000 bp to TSS) of *TFEB* and then performed the electrophoretic mobility shift assay (EMSA), a rapid and sensitive method detecting protein-nucleic acid interactions [32], to examine whether TRIM27 directly binds to the promoter region of *TFEB* gene. The result showed that the region ranging from –200 bp upstream to the TSS in *TFEB* was bound by TRIM27 directly (Figure 6A). We then analyzed the DNA-binding domain of TRIM27 using PredictProtein database (<https://predictprotein.org/>), and a total of two regions including amino acids 28–35 and 460–471 were identified in TRIM27 (Figure 6B). By deleting two potential DNA-binding domains of TRIM27 separately, we confirmed that the TRIM27 truncation with amino acids 460–471 deletion (TRIM27 Δ 460–471), but not the TRIM27 truncation with amino acids 28–35 deletion (TRIM27 Δ 28–35), largely lost its ability to bind to *TFEB* promoter (Figure 6B). Consistently, ChIP-qPCR assay confirmed that TRIM27 was highly enriched in the region ranging from –200 bp upstream to the TSS in *TFEB* promoter (Figure 6C). Accordingly, TRIM27-mediated transcription of *TFEB* was largely abolished by the deletion of the –200 bp to the TSS of the *TFEB* promoter or by the deletion of amino acids 460–471 of TRIM27 (Figure 6D). Thus, TRIM27 acts as a potential transcription activator of TFEB to promote TFEB expression, depending on the interaction of the –200 bp to the TSS promoter region of *TFEB* with the amino acids 460–471 of TRIM27. Given that CREB1 is the reported key transcription factor of *TFEB* [33], we further investigated whether TRIM27-mediated transcription of *TFEB* is dependent on CREB1. Through inhibiting CREB1-mediated gene transcription with *Creb1* shRNA or CREB1 inhibitor compound 3i (IC₅₀ = 0.081 ± 0.04 μM) [34] (Figure S6A), we found that the transcription of TRIM27 was not affected, while the promoting effect of TRIM27 on *TFEB* transcription was largely abolished in CREB1-knockdown macrophages (Figure 6E,F and S6B, C). These results suggest that CREB1 is required for TRIM27-mediated transcription of *TFEB*. Previous studies have reported that nuclear TRIM27 usually directly interacts with transcription factors to

regulate the gene transcription [35,36]. We thus detected whether TRIM27 directly interacts with CREB1 to induce gene transcription of *TFEB*. Co-immunoprecipitation and pull-down assays showed that TRIM27 directly interacted with CREB1 through its RET finger protein (RFP) domain (Figure 6G and S6D). We then performed luciferase reporter assays in HEK293T cells using pGL2-Basic reporter vector with the promoter region of *TFEB* gene inserted. Cells were co-transfected with the reporter plasmid and plasmid encoding wild-type TRIM27, E3 ligase activity-dead mutant of TRIM27 (TRIM27^{C16,31A}) [37,38], RING-B-box domain of TRIM27 (TRIM27 RB), Coiled-coil domain of TRIM27 (TRIM27 CC), RFP domain of TRIM27 (TRIM27 RFP), TRIM27 Δ 28–35 or TRIM27 Δ 460–471 (Figure S6E). The result showed that TRIM27, TRIM27^{C16,31A}, TRIM27 RFP and TRIM27 Δ 28–35, but not TRIM27 RB, TRIM27 CC or TRIM27 Δ 460–471, significantly induced the transcription of *TFEB* gene (Figure 6H). Collectively, TRIM27 interacts with CREB1 to promote *TFEB* gene transcription depending on its DNA-binding region (amino acids 460–471) and CREB1-interacting domain (RFP domain), which regulatory function is independent of the E3 ligase activity of TRIM27.

In order to further explore the detailed molecular mechanisms underlying TRIM27 binding to *TFEB* promoter and CREB1 to promote *TFEB* gene transcription, we performed a DNA-binding affinity assay to examine the effect of TRIM27 on CREB1 binding to the *TFEB* promoter. We found that TRIM27, but not TRIM27 Δ 460–471 or TRIM27 Δ RFP, significantly enhanced the affinity of CREB1 to bind to *TFEB* promoter (Figure 6I), suggesting that TRIM27 serves as an adaptor to promote the interaction between CREB1 and *TFEB* promoter region. Since the phosphorylation of CREB1 at Ser133 site (p-CREB1 S133) catalyzed by PRKA is required for CREB-mediated transcriptional activation in response to a variety of stimuli [39], we thus further investigated the contribution of TRIM27 to PRKA-catalyzed CREB1 phosphorylation. As expected, an obvious phosphorylation of CREB1 was detected in *Trim27*^{+/+} BMDMs, rather than in *trim27*^{-/-} BMDMs, during Mtb infection (Figure 6J). Moreover, the level of p-CREB1(S133) increased in a dose-dependent manner in the presence of TRIM27 (Figure 6K). We next sought to explore the mechanism by which TRIM27 promotes PRKA-mediated phosphorylation of CREB1. Confocal microscopy experiment and cell fractionation analysis showed that TRIM27 did not affect the nuclear translocation of CREB1 and PRKA upon Mtb infection (Figure S7 A – C). In vitro PRKA kinase activity assay further showed that TRIM27 had no effect on the kinase activity of PRKA (Figure S7D). Meanwhile, even though TRIM27 did not interact directly with PRKA (Figure S7E), the interaction between PRKA and CREB1 was significantly

immunoblotting (left). Right, the ratios of MAP1LC3-II:ACTB densitometry of quintuplicate samples was performed for quantification. (I) confocal microscopy analysis of autophagy in *Trim27*^{+/+} and *trim27*^{-/-} BMDMs. Left, Representative confocal images of fixed *Trim27*^{+/+} and *trim27*^{-/-} BMDMs. Cells were infected with mcherry-GFP-MAP1LC3-lentivirus for 24 h, and were then infected with Alexa Fluor™ 405-labeled mtb (blue) for 8 h. Uninfected cells were prepared as the negative control. Scale bars: 10 μm. Middle and right, the numbers of total MAP1LC3 puncta (middle) and the ratio of yellow:total MAP1LC3 puncta (right) from 50 cells for each biological replicate. Data are mean ± SEM ($n = 3$ replicates per group in A–G and I, $n = 5$ replicates per group in H). Statistical significance was determined using two-way ANOVA with Tukey's post-hoc test for (A–I). Results are representative of three independent experiments.

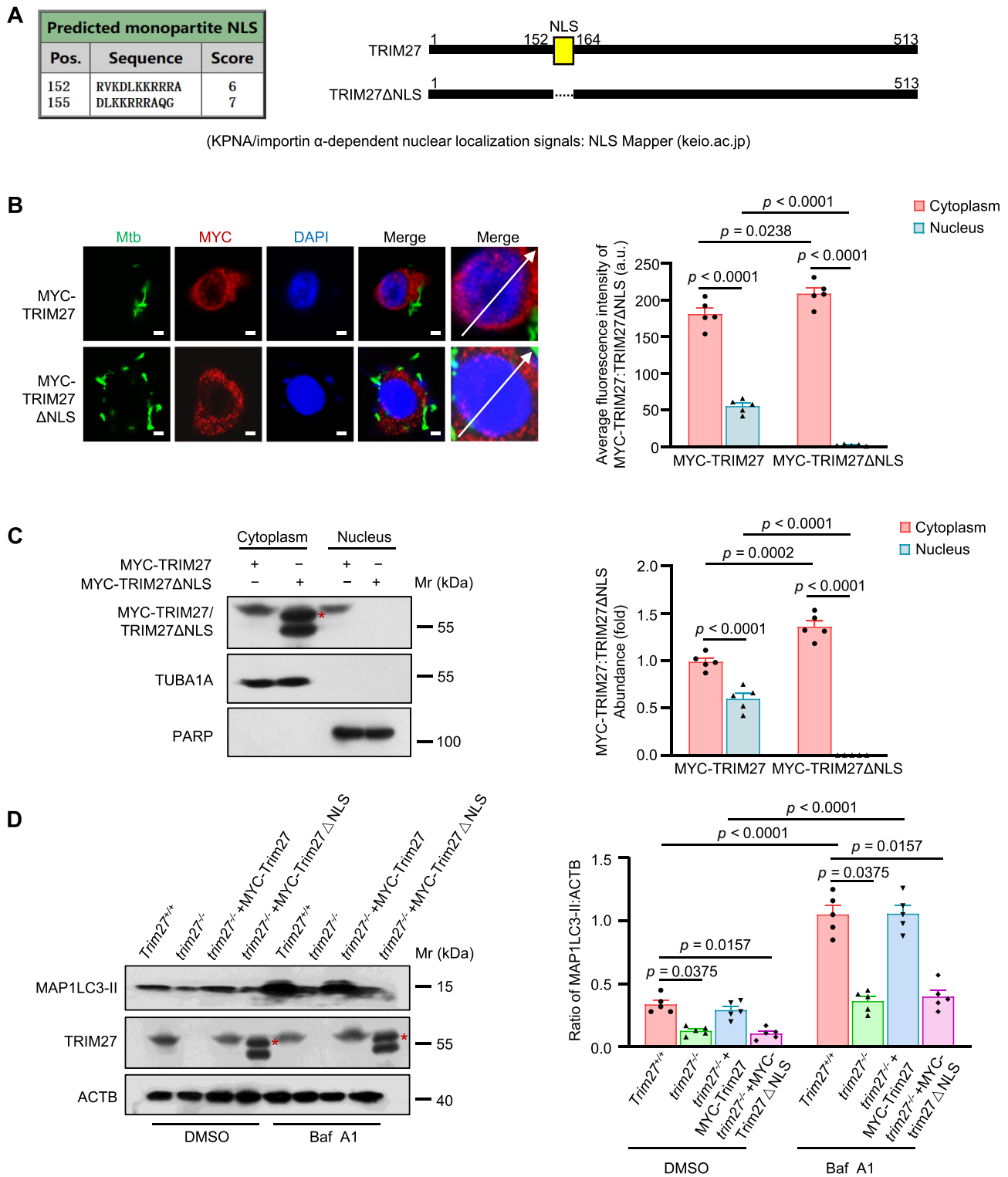


Figure 5. TRIM27 promotes autophagy activation depending on its nuclear localization. (A) schematic diagram representing the distribution region of nuclear localization signals (NLS) in TRIM27. The NLS were predicted with the cNLS mapper website. (B) confocal microscopy analysis of the nuclear localization of TRIM27 or TRIM27ΔNLS. Left, Representative confocal images of the colocalization of TRIM27 or TRIM27ΔNLS with the nucleus. RAW264.7 cells were transfected with vector encoding MYC-tagged TRIM27 or MYC-tagged TRIM27ΔNLS. After 24 h, transfected RAW264.7 cells were uninfected or infected with Alexa Fluor™ 488-labeled mtb (green) at a MOI of 5 for 8 h, and were then fixed and stained with the antibody against MYC-tag (red). Nuclei were stained with DAPI (blue). Scale bars: 5 μ m. Right, average fluorescence intensity of TRIM27 or TRIM27ΔNLS in the cytoplasm and nucleus. About 50 cells were counted and analyzed for each biological replicate. (C) immunoblotting of TRIM27, TUBA1A (loading control for the cytoplasm) and PARP (loading control for the nucleus) in the cytoplasm and nucleus in TRIM27- or TRIM27ΔNLS-complementing *trim27*^{-/-} BMDMs. Left, cells were transfected with MYC-TRIM27 or MYC-TRIM27ΔNLS for 24 h, and were then uninfected or infected with mtb for 8 h, followed by immunoblotting analysis. *: nonspecific bands. Right, the relative abundance of TRIM27 or TRIM27ΔNLS in the cytoplasm and nucleus. Densitometry of quintuplicate samples was performed for quantification. The relative abundance of TRIM27 or TRIM27ΔNLS in the cytoplasm and nucleus was calculated as the ratios of TRIM27:TUBA1A or TRIM27ΔNLS:TUBA1A and the ratios of TRIM27:PARP or TRIM27ΔNLS:PARP, respectively. (D) immunoblotting of MAP1LC3, TRIM27 and ACTB (loading control) in TRIM27- or TRIM27ΔNLS-complementing *trim27*^{-/-} BMDMs. Cells were infected as in (C), followed by immunoblotting analysis (left). *: nonspecific bands. Right, the ratios of MAP1LC3-II:ACTB. Densitometry of triplicate samples was performed for quantification. Data are mean \pm SEM ($n = 5$ replicates per group in B–D). Statistical significance was determined using two-way ANOVA with Tukey's post-hoc test for (B–D). Results are representative of three independent experiments.

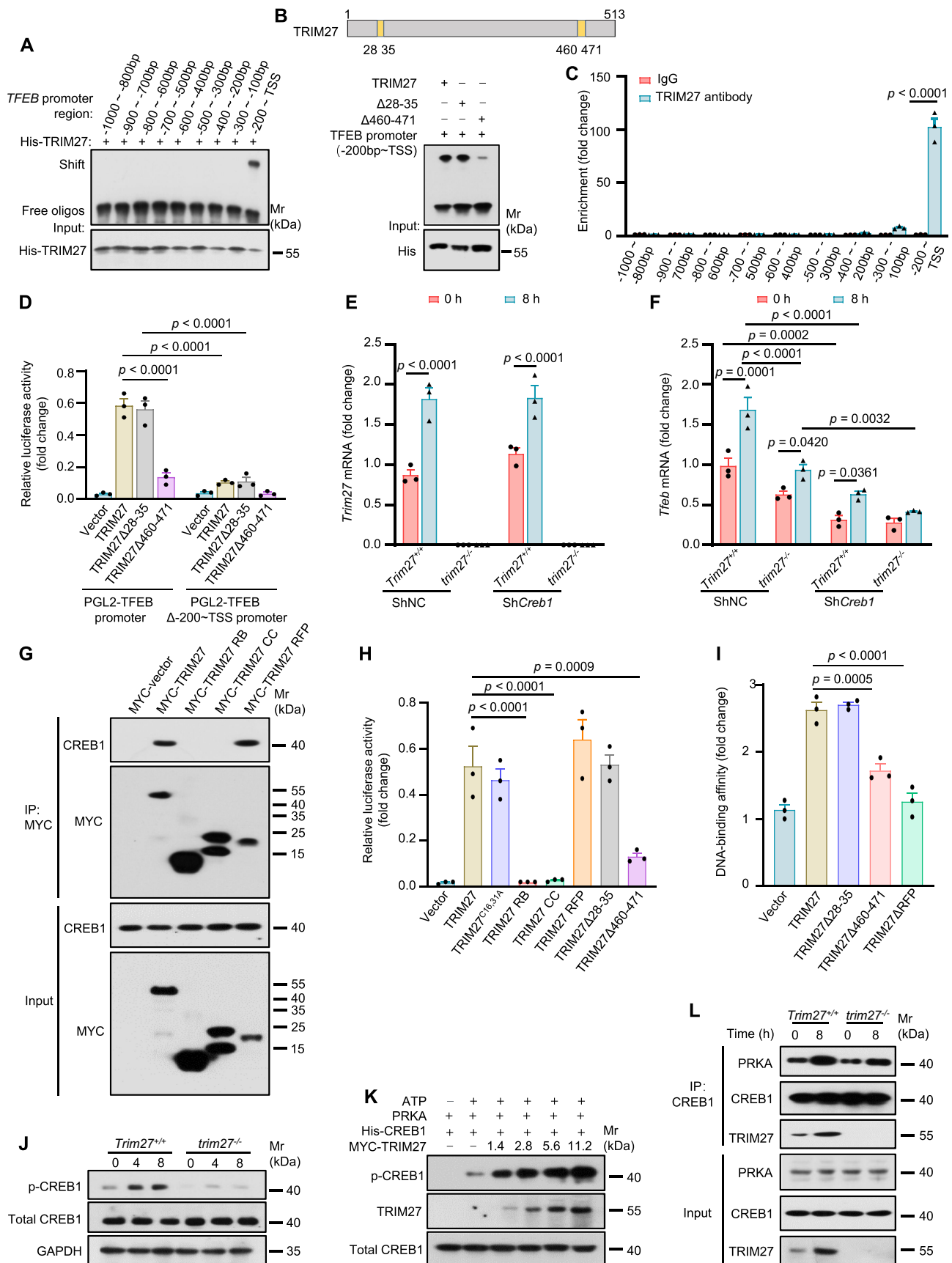


Figure 6. Nuclear TRIM27 functions as a transcription activator to enhance *TFEB* gene transcription during mtb infection. (A) electrophoretic mobility shift assay (EMSA) analysis of interactions between his-tagged TRIM27 and nine promoter fragments of *TFEB*. The promoter fragments of *TFEB* (10 nM) were amplified and incubated with 10 μ g of purified his-TRIM27. (B) EMSA analysis of interactions of his-tagged TRIM27 and its truncations with *TFEB* promoter fragment (-400 bp to the TSS) as in (A). (C) ChIP-qPCR analysis for the binding site of TRIM27 in the promoter of *TFEB* gene. ChIP assay was conducted using anti-TRIM27 rabbit antibody followed by qRT-PCR with specific primers for *TFEB* promoter fragments in PBMCs. Enrichment was calculated relative to the normal rabbit IgG control. (D) Luciferase

enhanced in the presence of TRIM27 during Mtb infection (Figure 6L). Consistently, RFP domain-deleted TRIM27 truncation (TRIM27 Δ RFP) caused a reduced phosphorylation level of CREB1 as compared to wild-type TRIM27 (Figure S7F). Collectively, TRIM27 interacts with CREB1 to promote the interaction of CREB1 with PRKA, thus enhancing the phosphorylation of CREB1 by PRKA. Altogether, TRIM27 functions as a transcription activator to enhance *TFEB* gene transcription through multiple effects. Specifically, TRIM27 not only interacts with both CREB1 and *TFEB* promoter to increase the binding affinity of CREB1 to the *TFEB* promoter, but also promotes PRKA-catalyzed CREB1 phosphorylation and activation, thereby leading to enhanced *TFEB* gene transcription.

CREB1 is essential for TRIM27 to enhance TFEB-mediated autophagy flux

To further determine whether CREB1 is required for TRIM27-mediated autophagy flux activation, we first examined the expression of autophagy-related genes in *Trim27*^{+/+} and *trim27*^{-/-} cells with or without *Creb1* shRNA or CREB1 inhibitor compound 3i treatment during Mtb infection. As shown in Figure 7A–G and Figure S8A–G, TRIM27 remarkably increased the transcription of autophagy-related genes, including *Map1lc3*, *Sqstm1*, *Ctsb*, *Atg5*, *Mcoln1*, *Lamp1* and *Lamp2*, upon Mtb infection, which phenomenon was largely abolished in CREB1-deficient macrophages. These results imply that the promoting effect of TRIM27 on autophagy-related gene expression is dependent on CREB1. Accordingly, *Trim27*^{+/+} BMDMs treated with compound 3i showed a significant decrease of the number of total MAP1LC3 puncta and an increase of the ratio of yellow:total puncta (Figure 7H), which indicate the attenuated autophagy induction and blocked autophagy flux, respectively. Consistently, the number of LAMP1 puncta that represents lysosomes also decreased both in *Trim27*^{+/+} and *trim27*^{-/-} BMDMs treated with compound 3i (Figure S8H). Finally, knockdown or inhibiting the activity of CREB1 enhanced the intracellular survival of Mtb both in *Trim27*^{+/+} and *trim27*^{-/-} cells (Figure 7I and S8I). Collectively, these results suggest that TRIM27 promotes TFEB-mediated autophagy activation depending on CREB1, thus suppressing pathogen intracellular survival.

TRIM27 promotes TFEB-mediated autophagy flux to enhance host anti-mtb immunity in vivo

To determine the role of TRIM27-mediated *TFEB* gene transcription and autophagy activation in host anti-Mtb immunity in vivo, we challenged *trim27*^{fl/fl} and *trim27*^{-/-Ly2z} mice by aerosol exposure with Mtb H37Rv strain to determine the bacterial loads and tissue pathology in the lungs or livers of the infected mice. Our data showed that Mtb infection could induce the transcription of *Trim27* in the lungs of *Trim27*^{fl/fl} mice (Figure 8A). Consistently, the transcription of *Tfeb* was markedly induced in the lungs of *Trim27*^{fl/fl} mice from 7 days post-infection, as compared with that in *trim27*^{-Ly2z} mice (Figure 8B). Based on the rationale that TRIM27 enhances autophagy flux to inhibit Mtb intracellular survival by promoting *TFEB* gene transcription, we then treated *Trim27*^{fl/fl} and *trim27*^{-Ly2z} mice with TFEB activator 1. Expectedly, TFEB activator 1 rescued the decreased expression of autophagy-related genes (including *Map1lc3* and *Atg5*) in macrophage cells from lungs of *trim27*^{-Ly2z} mice (Figure 8C,D and S9), as well as the reduced pathogen clearance in lungs and spleens of *trim27*^{-Ly2z} mice (Figure 8E,F). Consistently, TFEB activator 1 attenuated TRIM27 deficiency-mediated increase of cellular infiltrations and Mtb burden in lungs of Mtb-infected *trim27*^{-Ly2z} mice (Figure 8G–I). Thus, these results indicate that TRIM27 promotes *TFEB* gene transcription and the ensuing autophagy activation to enhance host anti-Mtb immunity in vivo, and TFEB activator 1 is a potentially attractive drug for alleviating the reduced ability of host defending against Mtb infection caused by TRIM27 deficiency.

In summary, our study demonstrates that TRIM27 nuclear localization increases upon Mtb infection in an NLS motif-dependent manner, followed by interacting with CREB1 and the *TFEB* promoter to increase the affinity of CREB1 to the *TFEB* promoter as well as promoting PRKA-catalyzed CREB1 phosphorylation and activation, thereby enhancing *TFEB* gene transcription, eventually leading to increased autophagy-related gene expression and autophagy activation to control Mtb intracellular survival (Figure 9). Thus, inducing *TFEB* gene transcription to enhance autophagy flux may serve as an effective strategy for the prevention and treatment of infectious diseases, such as TB, caused by TRIM27 deficiency.

Discussion

Until now, one of the leading causes of morbidity and mortality globally is infectious diseases, which are exacerbated by

reporter assay of the transcriptional regulation activity of TRIM27 or its truncations on the potential target gene *TFEB* or *TFEB* Δ -200bp~TSS in HEK293T cells. *TFEB* promoter- or *TFEB* Δ -200bp~TSS-pGL2-basic vector was co-transfected into HEK293T cells with 1 μ g of empty vector or vectors encoding full-length TRIM27 or its truncations. Resultant luciferase activities were expressed as relative luciferase activities normalized to the pRL-TK activity. (E and F) qRT-PCR analysis of *Trim27* mRNA (E) and *tfeb* mRNA (F) in *Trim27*^{+/+} and *trim27*^{-/-} cells stably expressing nontargeting control shRNA (shNC) or *Creb1*-targeting shRNA (sh*Creb1*). Cells were infected with mtb at a MOI of 5 for 0 or 8 h, and results are presented relative to those of the control gene *Gapdh*. (G) immunoprecipitation (IP) of CREB1 by MYC-tagged TRIM27 or its truncations in RAW264.7 cells. Cells were transfected with empty vector or vector encoding MYC-TRIM27 for 16 h and were then infected with mtb at a MOI of 5 for additional 8 h. Cells were lysed and immunoprecipitated with the antibody against MYC. (H) luciferase reporter assay of the transcriptional regulation activity of TRIM27 and its truncations on the potential target gene *TFEB* in HEK293T cells as in (D). (I) DNA-binding affinity of CREB1 in the presence of MYC-tagged TRIM27 or its truncations. (J) immunoblotting of p-CREB1, total CREB1 and GAPDH (loading control) in *Trim27*^{+/+} and *trim27*^{-/-} BMDMs. Cells were infected with mtb strains at a MOI of 5 for 0–8 h. (K) immunoblotting of TRIM27-mediated phosphorylation of CREB1 in vitro in the absence or presence of TRIM27. (L) IP of PRKA by CREB1 in *Trim27*^{+/+} and *trim27*^{-/-} BMDMs. Cells were infected as in (J), and were then lysed and immunoprecipitated with the antibody against CREB1. Data are mean \pm SEM ($n = 3$ replicates per group in C–F, H and I). Statistical significance was determined using two-way ANOVA with Sidak's multiple comparisons test for (C), two-way ANOVA with Tukey's post-hoc test for (D–F) and one-way ANOVA with Tukey's post-hoc test for (H and I). Results are representative of three independent experiments.

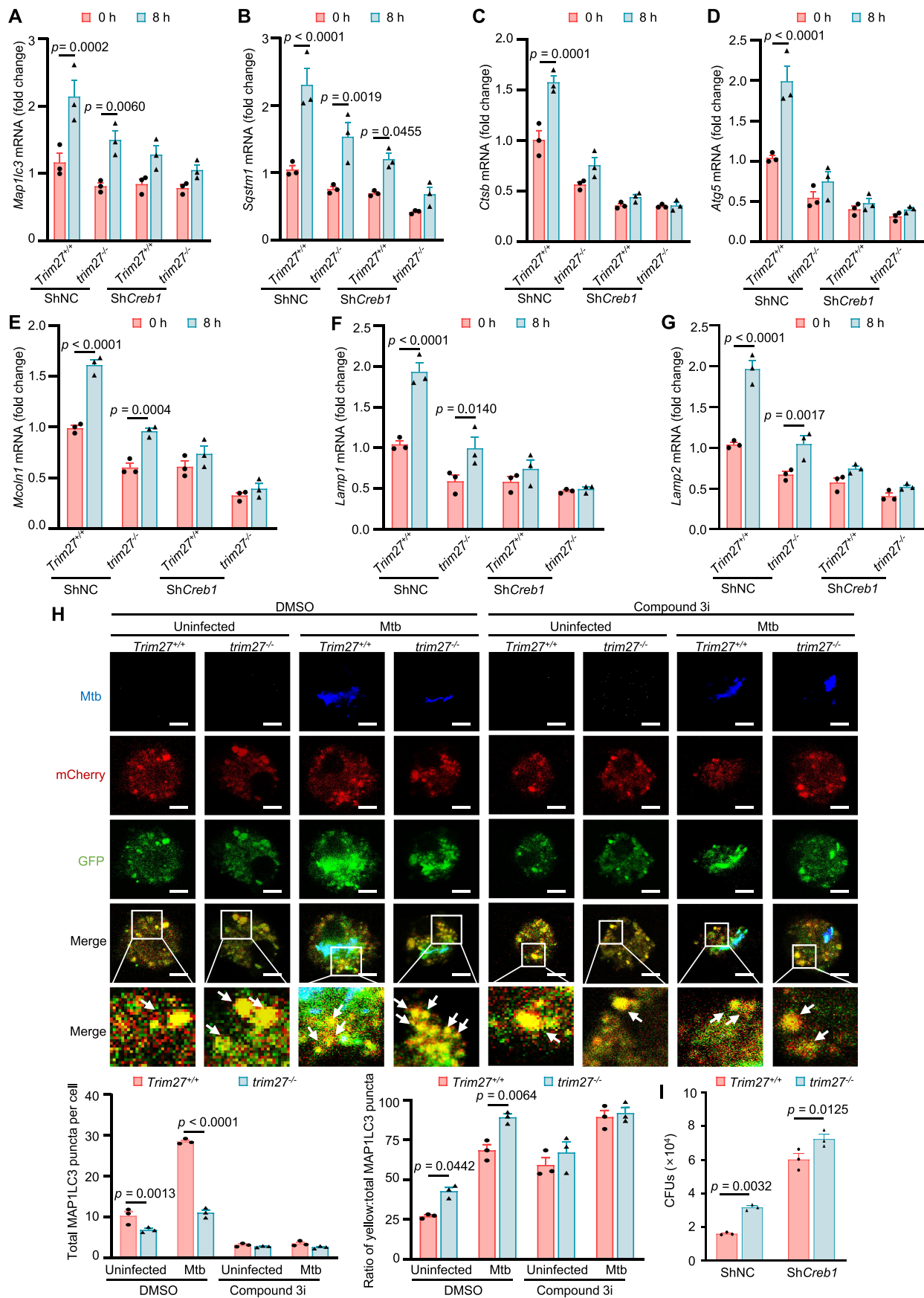


Figure 7. CREB1 is essential for TRIM27 to enhance TFEB-mediated autophagy flux. (A–G) qRT-PCR analysis of *Map1lc3* mRNA (A), *Sqstm1* mRNA (B), *ctzb* mRNA (C), *Atg5* mRNA (D), *Mcoln1* mRNA (E), *Lamp1* mRNA (F) and *Lamp2* mRNA (G) in *Trim27*^{+/+} and *trim27*^{-/-} cells stably expressing shNC or shCreb1. Cells were infected with mtb at a MOI of 5 for 0 or 8 h, and results are presented relative to those of the control gene *Gapdh*. (H) confocal microscopy analysis of autophagy in *Trim27*^{+/+} and *trim27*^{-/-} BMDMs with or without compound 3i treatment. Upper, Representative confocal image of fixed *Trim27*^{+/+} and *trim27*^{-/-} BMDMs. Cells were infected with

the widespread emergence of drug-resistant pathogens that challenge the healthcare infrastructure globally with economic consequences [40]. The host and pathogen have coexisted for eons and both of them have evolved diverse mechanisms to either adapt to or antagonize each other, and the interactions between them determine the outcomes of the infection. Understanding these evolutionary interactions and their impact on pathogen clearance or host pathology will provide insights into rational development of new therapeutics that favor enhancing a host protective response. It is well known that hosts have developed several strategies to recognize and restrict pathogen infection. Upon viral infection, a range of host factors, including many TRIM proteins, have been found to play critical roles in antagonizing viral invasion and replication [41], which provides key targets for the development of new host-directed antiviral infection therapies. Recently, several TRIM proteins (including TRIM14, TRIM16, TRIM22 and TRIM32) have been reported to be involved in host defense against bacteria such as Mtb [14–17], indicating that TRIM proteins are potential targets for HDT against bacterial infections. We previously found that TRIM27 regulates the activation of host innate immune signaling pathways to limit the infection of *M. bovis* BCG and *M. smegmatis* [19]. Here, we further revealed TRIM27 as a previously unrecognized host protective factor against Mtb. Specifically, upon Mtb infection, TRIM27 enters host cell nucleus, where it binds to *TFEB* gene promoter and interacts with the transcription factor CREB1, thus increasing the affinity of CREB1 to *TFEB* gene promoter and promoting PRKA-catalyzed CREB1 phosphorylation and activation, thereby enhancing *TFEB* transcription as well as autophagy flux to eliminate pathogens.

Autophagy is an emerging anti-infection innate immune mechanism that is usually induced upon infection, and it allows the prompt degradation of invading pathogens within lysosomes. In the past 20 years, the identification of the main components of the autophagy core machinery, named ATG (autophagy related) proteins, has revealed key aspects involved in the formation of autophagosomes [42]. More recently, considerable efforts have been devoted to further elucidating the detailed regulatory mechanisms involved in this process, and the autophagy flux that leads to eventual cargo degradation has been found to be frequently modulated during pathogenic infections. Several recent studies have demonstrated that TRIM proteins are important modulators of virus-induced autophagy. For example, TRIM5/TRIM5 α was recently shown to act as a viral cargo receptor inducing autophagic degradation of viral components [43]. Also, TRIM23 facilitates TBK1 activation to phosphorylate SQSTM1, ultimately enhancing cargo recognition and inducing autophagic degradation of viral components [44]. However, regarding bacterial infection, previous studies on

the role of TRIM proteins in autophagy mainly focused on the autophagy induction step [14–16], while the whole picture of the autophagy flux regulation by the TRIM proteins remains largely unclear. Here, we demonstrate that TRIM27 acts as a critical host factor promoting autophagy flux during Mtb infection, TRIM27 not only promotes autophagy induction to sequester pathogens in autophagosomes, but also enhances the autophagy flux to achieve eventual pathogen clearance. It is worth mentioning that a few studies have demonstrated the regulatory functions of TRIM27 on host autophagy under non-infection conditions. For example, one previous study reported that TRIM27 inhibits starvation-induced autophagy through impacting the ULK1 complex in a manner dependent on its E3 ubiquitin ligase activity [28], and another study showed that TRIM27 facilitates starvation-induced mitophagy through recruiting active TBK1 to the mitochondria in a manner dependent on its coiled-coil region [29]. Thus, TRIM27 plays pleiotropic roles in autophagy regulation depending on its specific domains or activities under different circumstances. Taken together, previous observations together with our findings indicate that TRIM27 regulates autophagy pathways in a disease-dependent manner, thus exerting disease-specific immune regulatory functions.

Transcriptional and epigenetic events play important roles in autophagy flux regulation upon stress stimuli [45], and various transcription regulators have been shown to regulate the expression of autophagy-related genes, including TFEB [21,46], a member of the MiTF/TFE family of leucine zipper transcription factors, plays as a critical regulator to promote autophagy flux. Under the static state, TFEB is phosphorylated by growth-factors/nutrients regulated kinases and is sequestered in the cytosol; upon stress stimulations, such as nutrient starvation, TFEB is dephosphorylated and translocated to nucleus to induce the expression of a variety of autophagy/lysosome-related genes [47–52]. Here, our data indicate that TRIM27 represents a newly identified protective factor against Mtb infection through directly binding to *TFEB* promoter and acts as a transcription activator to enhance *TFEB* gene transcription, thereby enhancing autophagy flux for pathogen clearance. Consistently, through analyzing clinical peripheral blood and lung tissues, we found that TB patients exhibit lower expression of TRIM27 as compared to healthy controls, suggesting that the defective expression of TRIM27 May predict TB development and progression. Thus, our findings suggest that TRIM27 is a potential biomarker that may serve as an indicator of TB status. In addition, for individuals with TRIM27 deficiency, enhancing *TFEB* transcription via targeting TRIM27-CREB1-TFEB axis or improving TFEB activity using compounds (such as TFEB activator 1) are potential effective HDTs for TB prevention and treatment.

mCherry-GFP-MAP1LC3-lentivirus for 24 h, and were then infected with Alexa FluorTM 405-labeled mtb (blue) at a MOI of 5 for 8 h with or without compound 3i treatment. Uninfected cells were prepared as the control. Scale bars: 10 μ m. Bottom, the numbers of total MAP1LC3 puncta (left) and the ratio of yellow:total MAP1LC3 puncta (right) from 50 cells for each biological replicate. (I) survival of mtb in *Trim27*^{+/+} and *trim27*^{-/-} cells stably expressing shNC or shCreb1. Data are mean \pm SEM ($n=3$ replicates per group in A–I). Statistical significance was determined using two-way ANOVA with Tukey's post-hoc test for (A–I). Results are representative of three independent experiments.

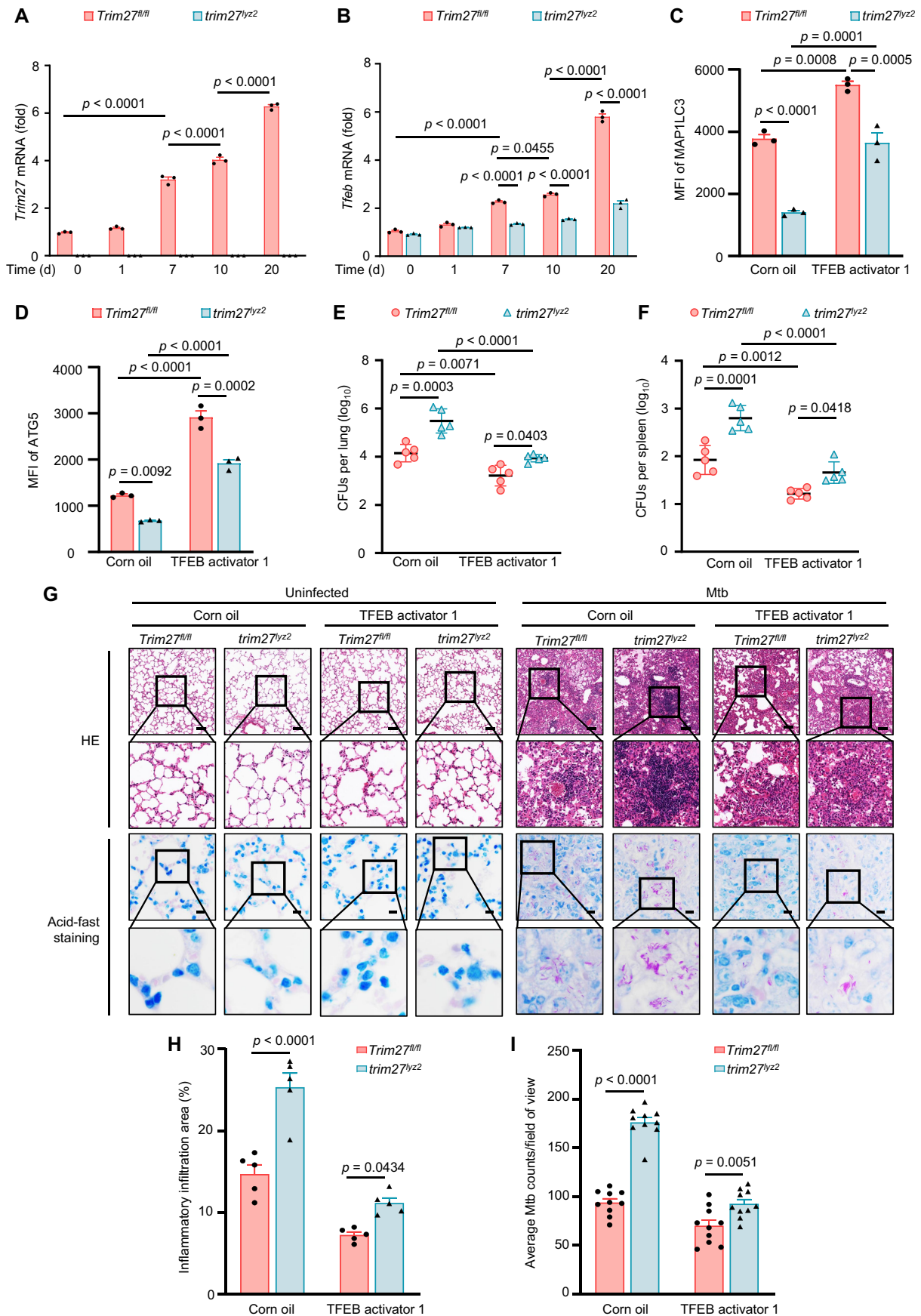


Figure 8. TRIM27 promotes TFEB-mediated autophagy flux to enhance host anti-mtb immunity in vivo. (A and B) qRT-PCR analysis of *Trim27* mRNA (A) and *Tfeb* mRNA (B) in the lungs of *Trim27^{fl/fl}* and *trim27^{lyz2}* mice infected with mtb at the indicated time points. (C and D) the MFI of MAP1LC3 (C) and ATG5 (D) in lung macrophages. The *Trim27^{fl/fl}* and *trim27^{lyz2}* mice were infected with mtb and treated with oil or TFEB activator 1 for 7 days, and the lungs were harvested for analysis by FACS. (E and F) bacterial loads of mtb in the lungs (E) and spleens (F) of *Trim27^{fl/fl}* and *trim27^{lyz2}* mice. Mice were infected and treated as in (C). (G)

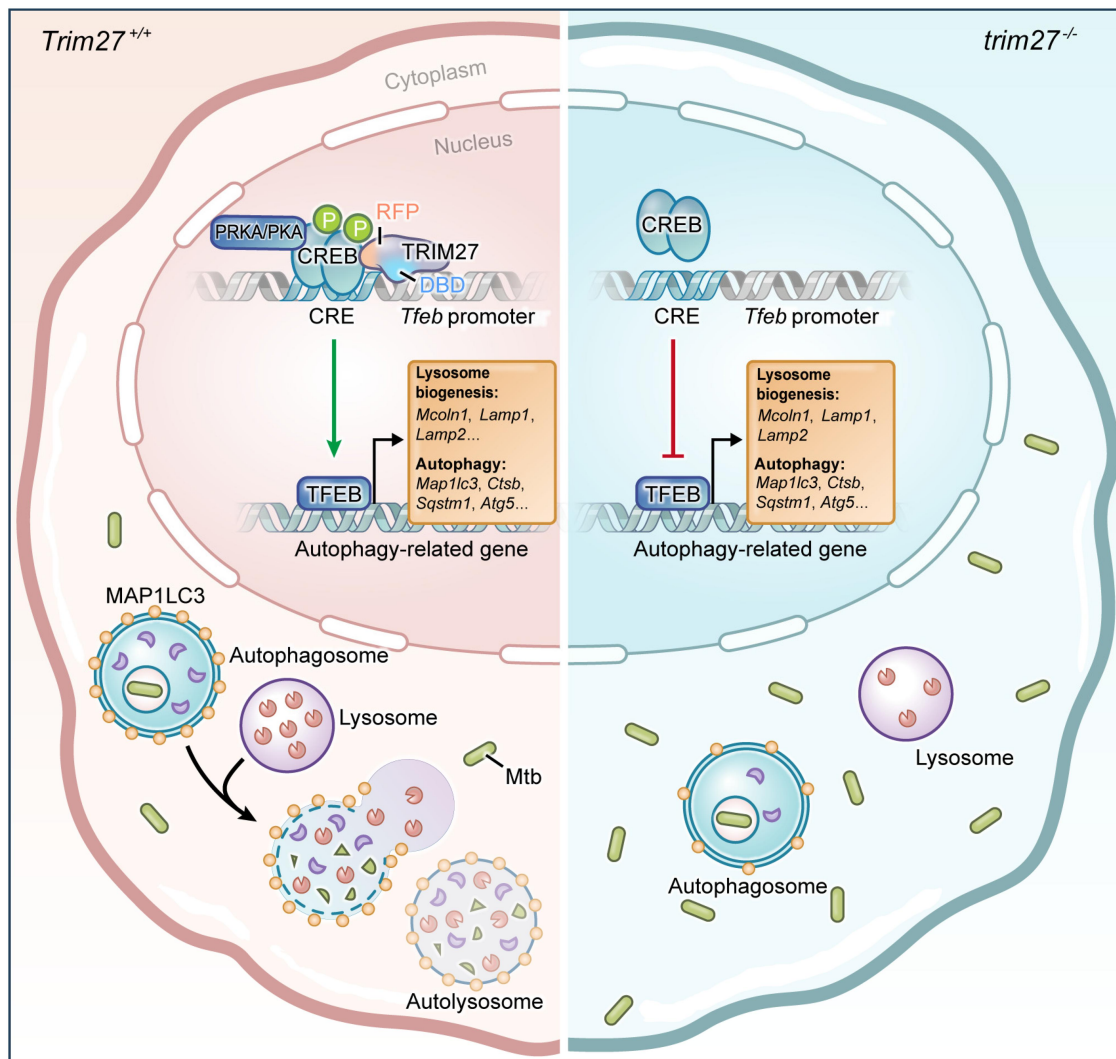


Figure 9. The schematic model showing that nuclear TRIM27 enhances *TFEB* transcription to promote autophagy flux and Mtb clearance. Briefly, during Mtb infection, nuclear TRIM27 increases and interacts with *TFEB* promoter and CREB1, followed by enhancing CREB1-*TFEB* promoter binding affinity and promoting phosphorylation of CREB1 at Ser133 catalyzed by PRKA, thus promoting *TFEB* gene transcription and the ensuing autophagy-related gene expression and autophagy activation to accelerate the clearance of pathogenic bacteria.

Materials and methods

Ethics

All animal studies were approved by the Biomedical Research Ethics Committee of Institute of Microbiology, Chinese Academy of Sciences (SQIMCAS2015004). HC and TB donors were recruited from Beijing Chest Hospital, and the study was approved by the Ethics Committee of Beijing Chest Hospital, Capital Medical University (2018KY41). Informed consent was obtained from all individual participants included in the study.

Donors

TB patients were diagnosed with significant symptoms of TB and a positive result of T-SPOT.TB test (a commercially

available IFNG release assay) [53,54], and were further confirmed by Mtb culture of respiratory specimens. The individual without a known history of exposure to Mtb was included as HC subjects based on a negative result of T-SPOT.TB test [53,55]. All participants aged ≥ 16 years old, and had no significant other medical histories such as human immunodeficiency virus (HIV) infection, cancers and diabetes. All participants were recruited from Beijing Chest Hospital. Information on HC and TB donors were provided in Table S1.

Mice

Lyz2/LyzM-Cre mice were from the Jackson Laboratory, *Trim27^{lox/flox}* (*Trim27^{fl/fl}*) mice were generated by

H&E and acid-fast staining of lung sections of *Trim27^{fl/fl}* and *trim27^{lyz2}* mice. Mice were infected and treated as in (C). (H and I) quantitation of inflammatory areas (H) and average mtb counts (I) in lung sections of *Trim27^{fl/fl}* and *trim27^{lyz2}* mice. Mice were infected and treated as in (C). Data are mean \pm SEM ($n = 3$ replicates per group in A–D, $n = 5$ replicates per group in E, F and H, $n = 10$ replicates per group in I). Statistical significance was determined using two-way ANOVA with Tukey's post-hoc test for (A–F, H and I). Results are representative of one experiment with two independent biological replicates.

Biocytogen (Beijing, China) using the CRISPR-Cas9 system. Both *Lyz2-Cre* mice and *Trim27^{fl/fl}* mice were in C57BL/6 genetic background. *Trim27^{fl/fl}* mice were first crossed with *Lyz2-Cre* mice. The F1 *trim27^{fllox/+}-Lyz2-Cre* mice then crossed with *Trim27^{fl/fl}* mice to generate *Trim27^{fllox/fllox}-Lyz2-Cre* (*trim27^{-/-}*) mice that lacked *Trim27* in myeloid cell lineage. All mice were housed and bred in a specific pathogen-free (SPF) facility on the basis of standard humane animal husbandry protocols, which were approved by the animal care and use committee of the Institute of Microbiology (Chinese Academy of Sciences). All experimental protocols were performed in accordance with the instructional guidelines of the China Council on Animal Care, and were approved by the Biomedical Research Ethics Committee of the Institute of Microbiology, Chinese Academy of Sciences, and the Beijing Chest Hospital, Capital Medical University (SQIMCAS2015004).

Bacterial strains and plasmids

E. coli DH5 α and BL21 were grown in flasks using lysogeny broth medium at 37°C with antibiotic selection for genetic manipulations or protein expression. Mtb H37Rv strain (ATCC 27,294) was grown in Middlebrook 7H9 (BD Biosciences 271,310) broth supplemented with 10% oleic acid-albumin-dextrose-catalase (OADC; Hopebio, HB6271a) and 0.05% Tween-80 (Sigma-Aldrich, 9005-65-6), or on Middlebrook 7H10 (BD Bioscience 262,710) agar supplemented with 10% OADC. For protein expression in mammalian cells, TRIM27 and its mutants were cloned into pcDNA6A (with MYC-tag) (Invitrogen, V22120) or pEGFP-N1 (with GFP-tag) vector (Clontech, 6085-1), *CREB1* was cloned into p3 \times Flag-CMV14 (with Flag-tag) vector (Sigma-Aldrich, E7908). Bacterial expression plasmids were constructed by cloning the cDNA of *TRIM27* or *CREB1* into pET30a (with His₆-tag) vector (Novagen 69,909). All the plasmids were sequenced at the Beijing Genomics Institute (BGI) for verification. All of the strains, plasmids and primers used in this study were detailed in Table S2.

Antibodies and reagents

All antibodies were used according to the manufacturer's instructions. The following commercial antibodies used in this study were as follows: anti-TRIM27 (Immuno-Biological Laboratories 18,791; 1:500 for immunoblots, 1:100 for immunofluorescence, 1:50 for chromatin immunoprecipitation), anti-Flag (Cell Signaling Technology 14,793; 1:1,000 for immunoblots), anti-MAP1LC3 (MBL Beijing Biotech Co., Ltd., M16-3; 1:3,000 for immunoblots), anti-LAMP1 (Abcam, ab24170; 1:200 for immunofluorescence), anti-GAPDH (Santa Cruz Biotechnology, sc -25,778; 1:4,000 for immunoblots), anti-CREB1 (Cell Signaling Technology, 9197; 1:1,000 for immunoblots, 1:250 for immunoprecipitation), anti-p-CREB1 (Abcam, ab32096; 1:4,000 for immunoblots), anti-PRKA/PKA (Cell Signaling Technology, 4782, 1:1,000 for immunoblots), anti-ATG5 (Cell Signaling Technology, 2630; 1:1,000 for immunoblots), anti-MYC (Cell Signaling Technology, 2276; 1:1,000 for immunoblots, 1:100 for immunofluorescence), anti-ACTB

(Sigma-Aldrich, A2228; 1:1,000 for immunoblots), anti-His (Cell Signaling Technology 12,698; 1:1,000 for immunoblots), anti-TUBA4A/TUBA1A/ α -Tubulin (Sigma-Aldrich, T6199; 1:4,000 for immunoblots), anti-PARP (Cell Signaling Technology, 9542; 1:1,000 for immunoblots), anti-TFEB (ABclonal Technology, A7311; 1:1,000 for immunoblots), anti-ULK1 (ABclonal Technology, A8529; 1:1,000 for immunoblots), anti-TOMM20 (ABclonal Technology, A19403; 1:1,000 for immunoblots), anti-TBK1 (Cell Signaling Technology, 3504; 1:1,000 for immunoblots), anti-p-TBK1 (Cell Signaling Technology, 5483; 1:1,000 for immunoblots), anti-p-ATG13 (Ser318) (Novus Biologicals, NBP2-19127SS; 1:1,000 for immunoblots), HRP-labeled goat anti-rabbit IgG (ZSGB Biotech, ZB-2306; 1:10,000 for immunoblots), HRP-labeled goat anti-mouse IgG (ZSGB Biotech, ZB-2305; 1:10,000 for immunoblots), anti-human CD3-PE/Cyanine7 (Biolegend 317,333; 1:200 for flow cytometry), anti-human CD4-FITC (Biolegend 300,506; 1:200 for flow cytometry), anti-human CD8-PerCP (Biolegend 980,916; 1:200 for flow cytometry), anti-human CD19-Brilliant Violet 421 (Biolegend 302,234; 1:200 for flow cytometry), anti-human NCAM1/CD56-Alexa Fluor700 (Biolegend 318,316; 1:200 for flow cytometry), anti-human PTPRC/CD45-PE (Biolegend 147,711; 1:200 for flow cytometry), anti-human CD14-Brilliant Violet 785 (Biolegend 301,840; 1:200 for flow cytometry), anti-mouse ITGAM/CD11b-Brilliant Violet 605 (Biolegend 101,237; 1:200 for flow cytometry), anti-mouse ADGRE1/F4/80-PerCP (Biolegend 123,125, 1:200 for flow cytometry). For antibody labeling, ReadILink™ Rapid iFluor™ 594, 488 and 647 Antibody Labeling Kits were purchased from AAT Bioquest (1230, 1255 and 1235, respectively). Molecular probes Alexa Fluor™ 488 (Invitrogen, A20000) and Alexa Fluor™ 405 (Invitrogen, A30000) were used for bacteria staining [56]. PRKACA/cAMP-dependent Protein Kinase catalytic subunit was purchased from New England Biolabs (P6000). LysoTracker was purchased from Invitrogen (L7528).

Cell culture and transfection

HEK293T cells (American Type Culture Collection, CRL-3216), the human monocytic cell line U937 cells (American Type Culture Collection, CRL-1593.2) and RAW264.7 cells (American Type Culture Collection, TIB-71) were used in this study. HEK293T and RAW264.7 cells were cultured in Dulbecco's modified Eagle's medium (DMEM; Invitrogen, C11995500BT) with 10% fetal bovine serum (FBS; Gibco 16,000-044). U937 cells were maintained in RPMI 1640 medium (Gibco, C11875500BT) with 10% FBS. Cells were cultured at 37°C in a humidified 5% CO₂ incubator. In all related experiments, U937 cells were differentiated into adherent macrophage-like cells using 10 ng/mL Phorbol 12-myristate 13-acetate (PMA; Sigma-Aldrich, P1585), and transient transfection assays were performed using Lipofectamine 2000 (Invitrogen 11,668,019) according to the manufacturers' instructions.

Generation of knockout and knockdown cell lines

We generated *Trim27*^{-/-} RAW264.7 cells using the CRISPR-Cas9 gene-editing system. The CRISPR-Gold was used to design the sgRNA sequences targeting the *Trim27* gene (Table S2). The sgRNA was cloned into pSpCas9(BB)-2A-GFP (Addgene 48,138; deposited by the Feng Zhang lab) as previously described [56]. The *atg5*^{+/+} and *atg5*^{-/-} RAW264.7 cells were transfected by recombinant pSpCas9(BB)-2A-GFP for 24 h. Single cell with green fluorescence was sorted with BD FACSAria III cell sorter (BD Biosciences) and was then identified by immunoblotting with anti-TRIM27 antibody. We designed the *Creb1*-specific shRNA sequences to silence expression of *Creb1* in *Trim27*^{+/+} and *trim27*^{-/-} RAW264.7 cells by BLOCK-iT™ RNAi Designer (Table S2). HEK293T cells were transfected with a mixture of pSIH1-H1-copGFP lentiviral vector (System Biosciences, SI501A-1) inserted with *Creb1* shRNA and packaging plasmids. After 48 h post-infection, viral supernatants were collected and filtered using a 0.45 µm syringe filter. *Trim27*^{+/+} and *trim27*^{-/-} RAW264.7 cells were infected with *Creb1* shRNA lentiviral particles for 24 h and were then identified by immunoblotting with anti-CREB1 antibody.

Isolation and differentiation of human monocyte-derived macrophages

PBMCs were isolated from venous blood from HC, LTBI or TB donors using Ficoll density gradient separation medium (DAKAWA 7,111,011) according to the manufacturer's instruction, and were then cultured in RPMI 1640 with 10% FBS for 7 days. Recombinant human macrophage colony-stimulating factor (CSF1/M-CSF; Invitrogen, PHC9504) was added on days 0, 2 and 4 to allow the differentiation of monocytes into macrophages.

Isolation of mouse bone marrow-derived macrophages

BMDMs were derived as described previously [56]. Briefly, bone marrow was irrigated from the tibia and femur of 8–12-week-old mice under sterile conditions. After lysis of red blood cells from bone marrow, the remaining cells were cultured in DMEM supplemented with 10% FBS, and 1% penicillin-streptomycin solution (Hyclone, SV30010). For differentiation into macrophages, the cells were cultured in DMEM with 10% FBS for 7 days. Recombinant murine CSF1/M-CSF (Dogesce, 315-02) was added on days 0, 2 and 4.

qRT-PCR analysis

Total RNA was extracted with FastPure Cell/Tissue Total RNA Isolation Kit (Vazyme, RC101-01). The total RNA was reverse-transcribed into cDNA using the Hieff First Strand cDNA Synthesis Super Mix (YEASEN, 11123ES60) and performed to qRT-PCR analysis with qPCR SYBR Green Master Mix (Low Rox Plus; YEASEN, 11202ES60) on ABI 7500 system (Applied Biosystems) as previously described [57]. Quantitative expression of the targeted gene was normalized

to *GAPDH* and data were analyzed by the $2^{-\Delta\Delta CT}$ method. Each experiment was performed in triplicates and repeated at least three times.

Flow cytometry

PBMCs from healthy volunteers or TB patients were blocked with anti-CD16/32 antibody for 30 min on ice. For frequency analyses of each immune cell subset, PBMCs were then stained with the indicated surface markers of monocytes, T cells, B cells and natural killer (NK) cells for 20 min at room temperature. For frequency analyses of macrophages in lungs from mice, the peripheral lung tissue was cut into small pieces with scissors, transferred into tubes and processed in digestion buffer (1 mg/mL of collagenase D [YEASEN, 40510ES76] and 0.1 mg/mL DNase I [YEASEN, 10608ES25] in Hanks' balanced salt solution [Beyotime Biotechnology, C0218]). Homogenized lungs were passed through 40-µm nylon mesh (JETBIOFIL, CSS013040) to obtain a single-cell suspension. Red blood cells were lysed using BD Pharm Lyse (BD Biosciences 555,899). The remaining cells were then stained with the indicated surface markers. Flow cytometric analysis was performed on a flow cytometer (Fortessa, BD Biosciences) and data were analyzed using FlowJo vx0.7 software.

Flow cytometry gating strategies were as follows: monocyte gating: FSC, SSC, PTPRC⁺, CD14⁺; CD4⁺ T cell gating: FSC, SSC, PTPRC⁺, CD3⁺, CD4⁺; CD8⁺ T cell gating: FSC, SSC, PTPRC⁺, CD3⁺, CD8⁺; B cell gating: FSC, SSC, PTPRC⁺, CD19⁺; NK cell gating: FSC, SSC, PTPRC⁺, CD3⁺, NCAM1⁺; macrophage gating: FSC, SSC, PTPRC⁺, ITGAM⁺, ADGRE1⁺; MAP1LC3⁺ macrophages: FSC, SSC, PTPRC/CD45⁺, ITGAM⁺, ADGRE1⁺, MAP1LC3⁺; ATG5⁺ macrophages: FSC, SSC, PTPRC⁺, ITGAM⁺, ADGRE1⁺, ATG5⁺.

Infection of macrophages

For BMDMs infection, Mtb in Middle brook 7H9 medium with 0.05% Tween-80 and 10% OADC enrichment were grown to an OD₆₀₀ of approximately 0.6. The bacterial pellet was then resuspended in DMEM medium with 0.05% Tween-80. The differentiated BMDMs were pretreated with 1 µM TFEB activator 1 (MedChemExpress, HY-135825) or 1 µM compound 3i (Selleck, 666-15) for 4 h and were then infected with Mtb at a multiplicity of infection (MOI) of 5. After 2 h, the media were discarded. Cells were washed for three times with 1 × PBS (137 mM NaCl, 2.7 mM KCl, 10 mM Na₂HPO₄, 2 mM KH₂PO₄, pH 7.4) to exclude noninternalized bacteria, and were then incubated with the fresh DMEM medium for additional 10 h.

Colony-forming unit (CFU) and immunoblotting analysis

For bacterial CFU counting, cells were washed with 1 × PBS for three times and lysed in 7H9 broth containing 0.05% SDS for 10 min. Several sets of serially gradient dilution of the lysates were prepared in 7H9 broth and then cultivated on 7H10 agar plates. The colonies were counted after 3–4 weeks. For immunoblotting analysis, cells were lysed in the Cell Lysis

Buffer for Western and IP (Beyotime Biotechnology, P0013). Proteins were separated by SDS-PAGE and transferred to polyvinylidene difluoride membranes (Millipore, IPVH00010). After incubation with primary and secondary antibodies, protein bands were detected using an Immobilon Western Chemiluminescent HRP Substrate (Millipore, WBKLS0500) and exposed to X-ray film. For quantifications, densitometry was performed using ImageJ 1.50e to evaluate the intensity of the immunoblotting band signals.

Separation of nuclear and cytoplasmic fractions

After Mtb infection, cells were washed and harvested in cold PBS. The cytoplasmic and nuclear fractions were then prepared with a Nuclear and Cytoplasmic Protein Extraction Kit (Beyotime Biotechnology, P0028) according to the manufacturer's instructions. Protein concentrations were determined by BCA Protein Assay Kit (Beyotime Biotechnology, P0011), and were then subjected to immunoblotting.

Immunofluorescence confocal microscopy

The bacteria were washed with Hanks' Balanced Salt Solution (Beyotime Biotechnology, C0218) containing 0.05% Tween-80 and resuspended in the buffer with adequate dye (Alexa FluorTM 488 or Alexa FluorTM 405) incubating for 30 min at 37°C. Then, the bacteria were washed and resuspended with DMEM medium containing 0.05% Tween-80. Cells were transfected with the indicated vectors or infected with the stained Mtb. Afterward, cells were washed with 1 × PBS for three times and fixed with 4% paraformaldehyde for 10 min, permeabilized with 0.5% Triton X-100 (Solarbio, T8200) in 1 × PBS for 10 min, blocked with 1% BSA (Biotopped, A6020A) in PBS for 1 h, stained with the indicated primary and secondary antibodies and labeled with DAPI. Then, confocal images were taken with Leica SP8 confocal system and processed with the Leica Application Suite Las X (v2.0.1.14392) program. For the image quantifications, approximately 50 cells were analyzed with Imaris 9.6 (Bitplane AG) for each biological replicate, and the data were shown as the mean ± SEM of three independent experiments.

Chromatin immunoprecipitation

ChIP experiments were carried out as described previously [58]. Briefly, cells were seeded in 100-mm dishes at 1×10^7 cells/dish then cross-linked with 1% formaldehyde for 10 min at room temperature, and quenched for 5 min with 0.125 M glycine. Afterward, cells were collected and lysed in 1% SDS lysis buffer supplemented with protease inhibitors cocktail (YEASEN, 20104ES03), sonicated with a 1:8-inch probe (5 s on:10 s off, 30 cycles, 25% of maxi power) by sonicator (Branson 550) to obtain genomic DNA fragments with an average size of 150–500 bp. ChIP was performed using anti-TRIM27 antibody (1:50) following the protocol provided by Millipore ChIP Assay kit (Millipore, 17–409) according to the manufacturer's introduction.

ChIP-seq analysis

The sequencing and generation of short DNA reads of immunoprecipitated samples were carried out with Illumina HiSeqTM 2500 at RIBOBIO Co. Ltd (Guangzhou, China). Binding sites were identified using MACS1.4 with a chromatin input library as the control data set. MACS assigns every candidate peak an enrichment p value, and those below a user-defined threshold p value (default 10^{-5}) are reported as the final peaks. The ratio between the ChIP-seq tag count and λ_{local} is reported as the fold enrichment.

Luciferase reporter assay

HEK293T cells seeded at 2.5×10^4 cells per well in a 12-well plate were cultured overnight. And then HEK293T cells were co-transfected with 1 μg pGL3-basic-*TFEB* promoter (−1000 bp to +49 bp from the TSS) vector or mock vector and 1 μg vector encoding MYC-TRIM27, MYC-TRIM27^{C16,31A}, MYC-TRIM27 RB, MYC-TRIM27 CC, MYC-TRIM27 RFP, TRIM27 Δ 28–35 or TRIM27 Δ 460–471. pRL-TK (100 ng) was used as an internal control. After 24 h, the cells were harvested and analyzed using the dual luciferase reporter assay kit (Promega, E1910).

Digestion of Mtb subcellular fractions

Proteins, DNA, RNA and glycans from logarithmic Mtb were digested as follows: For digestion of Mtb surface proteins, the bacilli were incubated with 100 $\mu\text{g}/\text{mL}$ proteinase K (YEASEN, 10401ES80) at 37°C for 30 min, and then protease inhibitor cocktail (YEASEN, 20124ES03) was used to terminate the reaction [56]. For digestion of Mtb intracellular proteins, DNA or RNA, the bacterial pellets were washed twice and resuspended in 50 mM Tris-HCl buffer (pH 7.5). Cells were then sonicated by Ultrasonic Homogenizer with an operating cycle of 3 s on and 7 s off at 200 W for 15 min on ice. The ultrasonic lysates were incubated with 100 $\mu\text{g}/\text{mL}$ proteinase K at 37°C for 15 min to remove intracellular proteins, and then protease inhibitor cocktail was used to terminate the reaction. DNA and RNA in the ultrasonic lysate were respectively digested with 20 U/mL DNase I (YEASEN, 10608ES25) containing 5 mM MgCl_2 and 100 $\mu\text{g}/\text{mL}$ RNase A (Beyotime Biotechnology, ST576). These reactions were respectively terminated using 2.5 mM EDTA at 65°C and using 2 U/ μL RNase Inhibitor (Beyotime Biotechnology, R0102) containing 1 mM DTT. For digestion of glycans, the bacterial cell wall was treated with 40 mM NaIO_4 (Adamas 013,474,148) to degrade saccharides, with 0.5 KU/mL mutanolysin (Sigma-Aldrich, SAE0092) to digest peptidoglycan, or with 60 U/mL α -mannosidase (Sigma-Aldrich, M7257) to transform lipomannan and lipoarabinomannan into mannoglycolipids for 24 h at 37°C. The digestion processes were terminated by denaturing the enzymes at 100°C for 5 min [59,60]. All digestive products were incubated with cells to detect *TRIM27* transcription levels.

DNA-binding affinity assay

TFEB promoter region (−400 bp to the TSS) was amplified by PCR and annealed according to the manufacturer's instructions (Beyotime Biotechnology, GS008). Flag-tagged CREB1 (10 μg) was incubated with 10 nM DNA oligos (*TFEB* promoter region) in the binding buffer (Beyotime Biotechnology, GS009) in the presence or absence of MYC-tagged TRIM27 or its truncations for 20 min at room temperature. The reaction mixtures were then incubated with Anti-FLAG® M2 Magnetic Beads (Millipore, M8823) at 4°C, followed by washing with PBS buffer for three times. The immunoprecipitated samples were analyzed by qRT-PCR (forward primer: 5'-cctgcacc-tactcctgaag-3', reverse primer: 5'-agttttcttctcctcag-3').

Electrophoretic mobility shift assays (EMSA)

TFEB promoter regions were amplified by PCR and biotinylated using the Biotin 3' End Labeling Kit (Beyotime Biotechnology, GS008) and annealed according to the manufacturer's instructions. His-tagged TRIM27 (10 μg) or its truncations (10 μg) was incubated with 10 nM biotin-labeled DNA oligos in the binding buffer (Beyotime Biotechnology, GS009) for 20 min at room temperature. The reaction mixtures were resolved on 1 mm-thick 15% non-denaturing polyacrylamide gels and transferred to HybondTM-N+ membranes (Beyotime Biotechnology, FFN13). The DNA oligomers were UV crosslinked to the membrane and the labeled probes were detected by the LightShift Chemiluminescent EMSA Kit (Beyotime Biotechnology, GS009).

Immunoprecipitation

For BMDMs, cells were infected with *Mtb* for 0–8 h and were lysed in the RIPA lysis buffer (Beyotime Biotechnology, P0013D) for 10 min at 4°C. Cell lysates were then incubated with the antibody against CREB1 (1:250) and protein A/G agarose (Santa Cruz Biotechnology, sc-2003) at 4°C, followed by washing with the RIPA lysis buffer. For HEK293T cells, cells were transfected with pcDNA6A empty vector or vector encoding MYC-tagged TRIM27 using Lipofectamine 2000. After 24 h, transfected HEK293T cells were lysed in the RIPA lysis buffer for 10 min at 4°C. Cell lysates were then incubated with the antibody against MYC-tag and protein A/G agarose at 4°C, followed by washing with the RIPA lysis buffer. The immunoprecipitated samples were analyzed by immunoblotting with the indicated antibodies.

In vivo and in vitro phosphorylation assay

For in vivo phosphorylation assay, *Trim27*^{+/+} and *trim27*^{-/-} BMDMs were infected with *Mtb* for 0–8 h and were then lysed in the RIPA lysis buffer for 10 min at 4°C. The cell lysates were normalized to a similar protein concentration and were subjected to immunoblotting with the antibody against p-CREB1 and total CREB1. For in vitro phosphorylation assay in Figure 6K, His-tagged CREB1 recombinant protein was expressed and batch purified from *E. coli* BL21 (DE3) using Ni-NTA beads (QIAGEN 30,230), and MYC-tagged

TRIM27 was obtained from HEK293T cells transfected with plasmid encoding MYC-TRIM27 using anti-MYC beads. About 5 μg of purified His-tagged CREB1 protein and 20,000 units PRKA were incubated at 30°C for 5 min in the presence or absence of 0–11.2 μg of MYC-tagged TRIM27 in kinase assay buffer containing 2 mM MnCl₂, 25 mM Tris-HCl, pH 7.5, 1 mM DTT and 100 μM ATP (Sigma-Aldrich, 20–306; pH 7.2). The reactions were stopped by adding 5 × SDS sample buffer and were then subjected to immunoblotting. For in vitro phosphorylation assay in Figure S7E and F, His-tagged TRIM27 and TRIM27ΔRFP recombinant proteins were expressed and batch purified from *E. coli* BL21 (DE3) using Ni-NTA beads. Flag-tagged CREB1 was obtained by immunoprecipitation from cell lysates transfected with vector encoding Flag-CREB1 using anti-Flag M2 beads. About 5 μg of purified Flag-tagged CREB1 protein and 20,000 units PRKA were incubated at 30°C for 5 min in the presence or absence of 11.2 μg of His-tagged TRIM27 (or 5.6 μg of His-tagged TRIM27ΔRFP) in kinase assay buffer containing 2 mM MnCl₂, 25 mM Tris-HCl, pH 7.5, 1 mM DTT and 100 μM ATP (Sigma-Aldrich, 20–306; pH 7.2). The reactions were stopped by adding 5 × SDS sample buffer, and the mixture was boiled for 10 min and subjected to immunoblotting.

Mouse model

Age-matched SPF male mice (approximately 6–8 weeks) were maintained under barrier conditions in a BSL-3 biohazard animal room. All the mice were housed under SPF conditions (12 h light/dark cycle, 50% relative humidity, between 25 and 27°C) with free access to food and tap water. For *Mtb* infection, mice were challenged by aerosol exposure with *Mtb* H37Rv using an inhalation device (Glas-Col, EK-IES) calibrated to deliver 100 CFUs of *Mtb*. Then, mice were orally fed with *TFEB* activator 1 (200 μg in 100 μL of corn oil) or corn oil (100 μL) (Solarbio, IC9000) daily for 20 days. At the indicated time points of infection, tissues (including lungs, livers and spleens) were harvested and sonicated in PBS for qRT-PCR, flow cytometry and CFU counting analyses, or were fixed in 10% formalin and embedded in paraffin for hematoxylin and eosin staining and Ziehl-Neelsen acid-fast staining. The tissue slices were collected by Leica CS2 and analyzed by SlideViewer (v2.5.0.143918), ImageScope (v12.3.3.7014) and ImageJ (v1.8.0) software. The sample size was based on empirical data from pilot experiments. No additional randomization or blinding was used to allocate experimental groups.

Statistical analysis

For in vitro study, investigators were not blinded to the sample identities during data collection since the readouts were quantitative and not prone to the subjective judgment of investigators. For in vivo study, mice experiments and statistical analysis were performed by independent researchers in a blinded manner. The quantified data with statistical analysis were performed using GraphPad Prism (v8.0) software. Unpaired two-sided Student's *t*-test, one-way ANOVA or two-way ANOVA analysis followed by multiple

comparisons was used for statistical analyses. Statistical significance and *p* value were mentioned in the figure legends and were indicated in the figures, respectively. At least three biological replicates were included. The data are presented as mean \pm SEM, and additional details about the statistical tests and numbers of samples are indicated in the corresponding figure legends.

Acknowledgements

We thank Tong Zhao (Institute of Microbiology, Chinese Academy of Sciences, Beijing) for helping with flow cytometry, Xiaolan Zhang (Institute of Microbiology, Chinese Academy of Sciences, Beijing) for helping with confocal microscopic analysis and Junfeng Hao (Core Facility for Protein Research, Institute of Biophysics, Chinese Academy of Sciences, Beijing) for helping with histological analysis.

Disclosure statement

No potential conflict of interest was reported by the author(s).

Funding

This work was supported by the National Key Research and Development Program of China [2022YFC2302900 to C.H.L. and J.W., 2021YFA1300200 to C.H.L., L.Z. and J.W.], the National Natural Science Foundation of China [82330069, 81825014 to C.H.L., 31830003 to C.H.L. and 82022041, 82372653 to J.W.], the Shenzhen Medical Research Funding [B2302035 to C.H.L.], the Strategic Priority Research Program of the Chinese Academy of Sciences [XDB29020000 to C.H.L.], the Open Project Program of CAS Key Laboratory of Pathogenic Microbiology and Immunology [CASPMI202206 to L.Z.], the CAS Project for Young Scientists in Basic Research [YSBR-010 to J.W.], and Youth Innovation Promotion Association CAS [Y2022036 to J.W.].

Data availability statement

The ChIP-seq data have been deposited in the Gene Expression Omnibus (GEO) database under accession code GSE237039. The authors declare that all other relevant data supporting the findings of this study are available within the article and its Supplementary Information files, or from the corresponding author on request. Source data are provided with this paper.

ORCID

Cui Hua Liu  <http://orcid.org/0000-0002-8035-7792>

Jing Wang  <http://orcid.org/0000-0001-5901-0797>

References

- [1] World Health Organization. Global Tuberculosis Report 2023. Geneva: World Health Organization; 2023. <https://www.who.int/teams/global-tuberculosis-programme/tb-reports/global-tuberculosis-report-2023>.
- [2] Tiberi S, Utjesanovic N, Galvin J, et al. Drug resistant TB – latest developments in epidemiology, diagnostics and management. *Int J of Infect Dis.* 2022;124(Suppl 1):S20–S25. doi: 10.1016/j.ijid.2022.03.026
- [3] World Health Organization. Global research agenda for antimicrobial resistance in human health. Geneva: World Health Organization; 2023. <https://www.who.int/publications/m/item/global-research-agenda-for-antimicrobial-resistance-in-human-health>.
- [4] Kaufmann SHE, Dorhoi A, Hotchkiss RS, et al. Host-directed therapies for bacterial and viral infections. *Nat Rev Drug Discov.* 2018;17(1):35–56. doi: 10.1038/nrd.2017.162
- [5] Kolloli A, Subbian S. Host-directed therapeutic strategies for tuberculosis. *Front Med.* 2017;4:171. doi: 10.3389/fmed.2017.00171
- [6] Wallis RS, O'Garra A, Sher A, et al. Host-directed immunotherapy of viral and bacterial infections: past, present and future. *Nat Rev Immunol.* 2023;23(2):121–133. doi: 10.1038/s41577-022-00734-z
- [7] Roy A, Kumari Agnivesh P, Sau S, et al. Tweaking host immune responses for novel therapeutic approaches against mycobacterium tuberculosis. *Drug Discov Today.* 2023;28(9):103693. doi: 10.1016/j.drudis.2023.103693
- [8] Ndlovu H, Marakalala MJ. Granulomas and inflammation: host-directed therapies for tuberculosis. *Front Immunol.* 2016;7:434. doi: 10.3389/fimmu.2016.00434
- [9] Hatakeyama S. TRIM family proteins: roles in autophagy, immunity, and Carcinogenesis. *Trends Biochem Sci.* 2017;42(4):297–311. doi: 10.1016/j.tibs.2017.01.002
- [10] Gushchina LV, Kwiatkowski TA, Bhattacharya S, et al. Conserved structural and functional aspects of the tripartite motif gene family point towards therapeutic applications in multiple diseases. *Pharmacol Ther.* 2018;185:12–25. doi: 10.1016/j.pharmthera.2017.10.020
- [11] Di Rienzo M, Romagnoli A, Antonioli M, et al. TRIM proteins in autophagy: selective sensors in cell damage and innate immune responses. *Cell Death Differ.* 2020;27(3):887–902. doi: 10.1038/s41418-020-0495-2
- [12] Giraldo MI, Hage A, van Tol S, et al. TRIM proteins in host Defense and viral pathogenesis. *Curr Clin Microbiol Rep.* 2020;7(4):101–114. doi: 10.1007/s40588-020-00150-8
- [13] Shen Z, Wei L, Yu Z-B, et al. The roles of TRIMs in antiviral innate immune signaling. *Front Cell Infect Microbiol.* 2021;11:628275. doi: 10.3389/fcimb.2021.628275
- [14] Chauhan S, Kumar S, Jain A, et al. Trims and Galectins Globally Cooperate and TRIM16 and galectin-3 co-direct autophagy in endomembrane damage homeostasis. *Dev Cell.* 2016;39(1):13–27. doi: 10.1016/j.devcel.2016.08.003
- [15] Romagnoli A, Di Rienzo M, Petruccioli E, et al. The ubiquitin ligase TRIM32 promotes the autophagic response to mycobacterium tuberculosis infection in macrophages. *Cell Death Dis.* 2023;14(8):505. doi: 10.1038/s41419-023-06026-1
- [16] Lou J, Wang Y, Zheng X, et al. TRIM22 regulates macrophage autophagy and enhances mycobacterium tuberculosis clearance by targeting the nuclear factor–multiplicity κ B/beclin 1 pathway. *J Cell Biochem.* 2018;119(11):8971–8980. doi: 10.1002/jcb.27153
- [17] Hoffpauir CT, Bell SL, West KO, et al. TRIM14 is a key regulator of the type I IFN response during mycobacterium tuberculosis infection. *J Immunol.* 2020;205(1):153–167. doi: 10.4049/jimmunol.1901511
- [18] Carthage L, Bergamaschi A, Luna JM, et al. Human TRIM gene expression in response to interferons. *PLoS One.* 2009;4(3):e4894. doi: 10.1371/journal.pone.0004894
- [19] Wang J, Teng JLL, Zhao D, et al. The ubiquitin ligase TRIM27 functions as a host restriction factor antagonized by Mycobacterium tuberculosis PtpA during mycobacterial infection. *Sci Rep.* 2016;6(1):34827. doi: 10.1038/srep34827
- [20] Kao CH, Su T-Y, Huang W-S, et al. TFEF- and TFE3-dependent autophagy activation supports cancer proliferation in the absence of centrosomes. *Autophagy.* 2022;18(12):2830–2850. doi: 10.1080/15548627.2022.2051880
- [21] Settembre C, Di Malta C, Polito VA, et al. TFEF links autophagy to lysosomal biogenesis. *Science.* 2011;332(6036):1429–33. doi: 10.1126/science.1204592
- [22] Pan B, Li J, Parajuli N, et al. The calcineurin-TFEF-p62 pathway mediates the activation of cardiac macroautophagy by Proteasomal Malfunction. *Circ Res.* 2020;127(4):502–518. doi: 10.1161/CIRCRESAHA.119.316007
- [23] Lopez A, Fleming A, Rubinsztein DC. Seeing is believing: methods to monitor vertebrate autophagy in vivo. *Open Biol.* 2018;8(10). doi: 10.1098/rsob.180106

- [24] Mauvezin C, Neufeld TP. Bafilomycin A1 disrupts autophagic flux by inhibiting both V-ATPase-dependent acidification and ca-P60A/SERCA-dependent autophagosome-lysosome fusion. *Autophagy*. 2015;11(8):1437–8. doi: [10.1080/15548627.2015.1066957](https://doi.org/10.1080/15548627.2015.1066957)
- [25] Wang L, Zhao C, Zheng T, et al. Torin 1 alleviates impairment of TFEB-mediated lysosomal biogenesis and autophagy in TGFBI (p.G623_H626del)-linked thiel-behnke corneal dystrophy. *Autophagy*. 2022;18(4):765–782. doi: [10.1080/15548627.2021.1955469](https://doi.org/10.1080/15548627.2021.1955469)
- [26] Zhao YG, Codogno P, Zhang H. Machinery, regulation and pathophysiological implications of autophagosome maturation. *Nat Rev Mol Cell Biol*. 2021;22(11):733–750. doi: [10.1038/s41580-021-00392-4](https://doi.org/10.1038/s41580-021-00392-4)
- [27] Song JX, Sun Y-R, Peluso I, et al. A novel curcumin analog binds to and activates TFEB in vitro and in vivo independent of mTOR inhibition. *Autophagy*. 2016;12(8):1372–89. doi: [10.1080/15548627.2016.1179404](https://doi.org/10.1080/15548627.2016.1179404)
- [28] Yang Y, Zhu Y, Zhou S, et al. TRIM27 cooperates with STK38L to inhibit ULK1-mediated autophagy and promote tumorigenesis. *EMBO J*. 2022;41(14):e109777. doi: [10.15252/embj.2021109777](https://doi.org/10.15252/embj.2021109777)
- [29] Garcia-Garcia J, Berge AKM, Overà KS, et al. TRIM27 is an autophagy substrate facilitating mitochondria clustering and mitophagy via phosphorylated TBK1. *FEBS J*. 2023;290(4):1096–1116. doi: [10.1111/febs.16628](https://doi.org/10.1111/febs.16628)
- [30] Kosugi S, Hasebe M, Tomita M, et al. Systematic identification of cell cycle-dependent yeast nucleocytoplasmic shuttling proteins by prediction of composite motifs. *Proc Natl Acad Sci USA*. 2009;106(25):10171–6. doi: [10.1073/pnas.0900604106](https://doi.org/10.1073/pnas.0900604106)
- [31] Kosugi S, Hasebe M, Entani T, et al. Design of peptide inhibitors for the Importin α/β Nuclear Import Pathway by activity-based profiling. *Chem Biol*. 2008;15(9):940–949. doi: [10.1016/j.chembiol.2008.07.019](https://doi.org/10.1016/j.chembiol.2008.07.019)
- [32] Hellman LM, Fried MG. Electrophoretic mobility shift assay (EMSA) for detecting protein-nucleic acid interactions. *Nat Protoc*. 2007;2(8):1849–1861. doi: [10.1038/nprot.2007.249](https://doi.org/10.1038/nprot.2007.249)
- [33] Seok S, Fu T, Choi S-E, et al. Transcriptional regulation of autophagy by an FXR-CREB axis. *Nature*. 2014;516(7529):108–111. doi: [10.1038/nature13949](https://doi.org/10.1038/nature13949)
- [34] Xie F, Li BX, Kassenbrock A, et al. Identification of a potent inhibitor of CREB-Mediated gene transcription with efficacious in vivo anticancer activity. *J Med Chem*. 2015;58(12):5075–87. doi: [10.1021/acs.jmedchem.5b00468](https://doi.org/10.1021/acs.jmedchem.5b00468)
- [35] Gibbs ZA, Reza, LC, Cheng, CC, et al. The Testis Protein ZNF165 Is a SMAD3 Cofactor That Coordinates Oncogenic TGFbeta Signaling In Triple-Negative Breast Cancer. *Elife*. 2020;9:e57679.
- [36] Kato T, Enomoto A, Watanabe T, et al. TRIM27/MRTF-B-Dependent integrin $\beta 1$ expression defines leading cells in cancer cell collectives. *Cell Rep*. 2014;7(4):1156–1167. doi: [10.1016/j.celrep.2014.03.068](https://doi.org/10.1016/j.celrep.2014.03.068)
- [37] Hasegawa N, Iwashita T, Asai N, et al. A RING finger motif regulates transforming activity of the rfp/ret fusion gene. *Biochem Biophys Res Commun*. 1996;225(2):627–31. doi: [10.1006/bbrc.1996.1221](https://doi.org/10.1006/bbrc.1996.1221)
- [38] Zurek B, Schoultz I, Neerinx A, et al. TRIM27 negatively regulates NOD2 by ubiquitination and proteasomal degradation. *PLoS One*. 2012;7(7):e41255. doi: [10.1371/journal.pone.0041255](https://doi.org/10.1371/journal.pone.0041255)
- [39] Naqvi S, Martin KJ, Arthur JS. CREB phosphorylation at Ser133 regulates transcription via distinct mechanisms downstream of cAMP and MAPK signalling. *Biochem J*. 2014;458(3):469–79. doi: [10.1042/BJ20131115](https://doi.org/10.1042/BJ20131115)
- [40] Islam T. Infectious diseases surveillance update. *Lancet Infect Dis*. 2022;22(7):952. doi: [10.1016/S1473-3099\(22\)00381-4](https://doi.org/10.1016/S1473-3099(22)00381-4)
- [41] Cloherty APM, Rader AG, Compeer B, et al. Human TRIM5 α : Autophagy Connects Cell-Intrinsic HIV-1 Restriction and innate immune sensor functioning. *Viruses*. 2021;13(2):320. doi: [10.3390/v13020320](https://doi.org/10.3390/v13020320)
- [42] Levine B, Kroemer G. Biological functions of autophagy genes: a disease perspective. *Cell*. 2019;176(1–2):11–42. doi: [10.1016/j.cell.2018.09.048](https://doi.org/10.1016/j.cell.2018.09.048)
- [43] Ribeiro CM, Sarrami-Forooshani R, Setiawan LC, et al. Receptor usage dictates HIV-1 restriction by human TRIM5 α in dendritic cell subsets. *Nature*. 2016;540(7633):448–452. doi: [10.1038/nature20567](https://doi.org/10.1038/nature20567)
- [44] Sparrer KMJ, Gableske S, Zurenski MA, et al. TRIM23 mediates virus-induced autophagy via activation of TBK1. *Nat Microbiol*. 2017;2(11):1543–1557. doi: [10.1038/s41564-017-0017-2](https://doi.org/10.1038/s41564-017-0017-2)
- [45] Parzych KR, Kliensky DJ. An overview of autophagy: morphology, mechanism, and regulation. *Antioxid Redox Signal*. 2014;3(3):460–73. doi: [10.1089/ars.2013.5371](https://doi.org/10.1089/ars.2013.5371)
- [46] Rocznik-Ferguson A, Petit CS, Froehlich F, et al. The transcription factor TFEB links mTORC1 signaling to transcriptional control of lysosome homeostasis. *Sci Signal*. 2012;5(228):ra42. doi: [10.1126/scisignal.2002790](https://doi.org/10.1126/scisignal.2002790)
- [47] Brady OA, Martina JA, Puertollano R. Emerging roles for TFEB in the immune response and inflammation. *Autophagy*. 2018;14(2):181–189. doi: [10.1080/15548627.2017.1313943](https://doi.org/10.1080/15548627.2017.1313943)
- [48] Chen M, Dai Y, Liu S, et al. TFEB Biology And Agonists At a Glance. *Cells*. 2021;10(2):333
- [49] Nnah IC, Wang B, Saqcenca C, et al. TFEB-driven endocytosis coordinates mTORC1 signaling and autophagy. *Autophagy*. 2019;15(1):151–164. doi: [10.1080/15548627.2018.1511504](https://doi.org/10.1080/15548627.2018.1511504)
- [50] Sha Y, Rao L, Settembre C, et al. STUB 1 regulates TFEB -induced autophagy-lysosome pathway. *EMBO J*. 2017;36(17):2544–2552. doi: [10.15252/embj.201796699](https://doi.org/10.15252/embj.201796699)
- [51] Napolitano G, Esposito A, Choi H, et al. mTOR-dependent phosphorylation controls TFEB nuclear export. *Nat Commun*. 2018;9(1):3312. doi: [10.1038/s41467-018-05862-6](https://doi.org/10.1038/s41467-018-05862-6)
- [52] Paik S, Kim JK, Chung C, et al. Autophagy: a new strategy for host-directed therapy of tuberculosis. *Virulence*. 2019;10(1):448–459. doi: [10.1080/21505594.2018.1536598](https://doi.org/10.1080/21505594.2018.1536598)
- [53] Chee CB, Barkham TMS, KhinMar KW, et al. Quantitative T-cell interferon-gamma responses to Mycobacterium tuberculosis-specific antigens in active and latent tuberculosis. *Eur J Clin Microbiol Infect Dis*. 2009;28(6):667–70. doi: [10.1007/s10096-008-0670-8](https://doi.org/10.1007/s10096-008-0670-8)
- [54] Wagstaff AJ, Zellweger JP. T-SPOT.TB: an in vitro diagnostic assay measuring T-cell reaction to Mycobacterium tuberculosis-specific antigens. *Mol Diagn Ther*. 2006;10(1):57–63. doi: [10.1007/BF03256443](https://doi.org/10.1007/BF03256443) discussion 64-5.
- [55] Herrera V, Perry S, Parsonnet J, et al. Clinical application and Limitations of Interferon- release assays for the diagnosis of latent tuberculosis infection. *Clin Infect Dis*. 2011;52(8):1031–1037. doi: [10.1093/cid/cir068](https://doi.org/10.1093/cid/cir068)
- [56] Chai Q, Wang X, Qiang L, et al. A Mycobacterium tuberculosis surface protein recruits ubiquitin to trigger host xenophagy. *Nat Commun*. 2019;10(1):1973. doi: [10.1038/s41467-019-09955-8](https://doi.org/10.1038/s41467-019-09955-8)
- [57] Wang J, Li B-X, Ge P-P, et al. Mycobacterium tuberculosis suppresses innate immunity by coopting the host ubiquitin system. *Nat Immunol*. 2015;16(3):237–45. doi: [10.1038/ni.3096](https://doi.org/10.1038/ni.3096)
- [58] Wang T, Ren Y, Liu R, et al. miR-195-5p suppresses the proliferation, migration, and invasion of oral squamous cell carcinoma by targeting TRIM14. *Biomed Res Int*. 2017;2017:1–13. doi: [10.1155/2017/7378148](https://doi.org/10.1155/2017/7378148)
- [59] Rimal B, Senzani S, Ealand C, et al. Peptidoglycan compositional analysis of mycobacterium smegmatis using high-resolution LC-MS. *Sci Rep*. 2022;12(1):11061. doi: [10.1038/s41598-022-15324-1](https://doi.org/10.1038/s41598-022-15324-1)
- [60] De P, Amin AG, Flores D, et al. Structural implications of lipoarabinomannan glycans from global clinical isolates in diagnosis of Mycobacterium tuberculosis infection. *J Biol Chem*. 2021;297(5):101265. doi: [10.1016/j.jbc.2021.101265](https://doi.org/10.1016/j.jbc.2021.101265)